Chemical Engineering Journal Advances 27 (2026) 101255

Contents lists available at ScienceDirect

Chemical Engineering Journal Advances

journal homepage: www.sciencedirect.com/journal/chemical-engineering-journal-advances

Enhancing methanol synthesis from CO_2: A comparison of interstage product separation via condensation and membranes

Matthias Schiedeck [a,b,*], Hannes Stadler [a], Andreas Peschel [a,b]

[a] Forschungszentrum Jülich GmbH, Institute for a sustainable Hydrogen Economy (IHE), Jülich, Germany
[b] RWTH Aachen University, Aachener Verfahrenstechnik, Process and Plant Engineering for Chemical Hydrogen Storage, Aachen, Germany

ARTICLE INFO

Keywords:
Methanol synthesis
Multistage reactor
Polymer membranes
Membrane separation
Interstage condensation

ABSTRACT

Interstage product separation is a practical strategy to address challenges related to the equilibrium limitation in CO_2-based methanol synthesis. While many studies assess intensification strategies at the reactor level, this work examines the process-wide implications of interstage condensation and membrane separation units in comparison to the performance of a single-stage condensation reference. Interstage condensation increases carbon efficiency by 3 to 12 percentage points over the reference without increasing power demand. Gains are most pronounced for the first additional stage at low pressures and diminish with both increasing stages and pressure. The required cooling and reheating before and after the condensation steps increases total heat transfer demand by 13 to 83% over the single-stage reference, concentrated close to the reaction stages. Membrane-based interstage separation operates at elevated temperatures compatible with low-cost polymer membranes, avoiding this thermal burden near the reaction stages. Under more aggressive separation conditions, carbon efficiency can exceed the condensation process (e.g. 98.9% vs. 98.5% at 80 bar process pressure and three stages), but sweep handling increases total heat duty (+38%) and compressor power demand (+11%). Under milder separation conditions, compressor power demand approaches the condensation case (+2%) and total heat duty is reduced (−8%), but carbon efficiency drops to 98.3%. Interstage condensation emerges as the more robust and conceptually simpler option, although its operational advantages over the single-stage reference must be weighed against additional investment and equipment-related complexity.

1. Introduction

In the context of a sustainable hydrogen economy, hydrogen-containing bulk chemicals like methanol are taking on an additional application as energy vectors, e.g. as carrier molecules for intercontinental transport of hydrogen or directly as a fuel [1,2]. This development comes along with challenges of changing boundary conditions of these well-established processes, mostly associated with the replacement of their conventional fossil feedstock such as natural gas or coal [3].

CO_2 as an alternative carbon source for methanol synthesis, e.g. captured from industrial waste streams, has been discussed for over 20 years [4] and is strongly rooted in George Olah's pioneering concept of the *methanol economy* [5]. Compared to NG-based synthesis gas, the thermodynamics of CO_2-based methanol synthesis is characterized by increased water production and lower methanol yield [4]. Increased water production is a challenge for conventional $Cu/ZnO/Al_2O_3$ catalysts as it accelerates catalyst sintering, resulting in faster deactivation [6]. Moreover, the lower conversion rate leads to an increased recycle stream, which in turn requires larger equipment and leads to higher operating costs [7]. In addition to the development of novel catalysts or the adaptation of conventional catalysts towards water-resistance [8,9], in-situ or intermediate separation of the reaction products could help to overcome this hurdle in CO_2-based methanol synthesis.

In-situ or intermediate product separation tackles the issue of the well-known equilibrium limitation in methanol synthesis, which limits the possible single-pass conversion and is industrially solved by recycling unconverted reactants. Overcoming the equilibrium limitation by selective product separation can be achieved by a variety of different separation principles: adsorption, absorption, condensation, or membrane separation.

Studies dealing with the adsorption-enhanced MeOH synthesis consistently report higher single-pass conversion and methanol yield in comparison to the conventional process, e.g., Arora et al. [10] using NaX zeolites, and Bayat et al. [11] using zeolite 4A. However, due to the limited capacity of these solid adsorbents, the effect of product separation diminishes once saturation is reached [12]. As a result,

* Corresponding author at: Forschungszentrum Jülich GmbH, Institute for a sustainable Hydrogen Economy (IHE), Jülich, Germany.
E-mail address: m.schiedeck@fz-juelich.de (M. Schiedeck).

https://doi.org/10.1016/j.ceja.2026.101255
Received 23 March 2026; Received in revised form 7 May 2026; Accepted 17 May 2026
Available online 25 May 2026

adsorption-enhanced process concepts inherently need regeneration of the adsorbents. Typically, this requires either challenging handling of moving solids for ex-situ regeneration of the adsorbent [11] or discontinuous production for periodic in-situ regeneration cycles [10], both rendering the processes complex and prone to disturbances [13].

Similar improvements in conversion and methanol yield have been reported for absorption-enhanced concepts, which involve selective removal of reaction products using specialized liquids. Examples include interstage absorption with tetraethylene glycol dimethyl ether [14] and in-situ absorption using alkali salt-doped ionic liquids [15]. However, introducing an additional working fluid adds significant process complexity and imposes potentially conflicting requirements on the absorbent, namely high capacity and selectivity, low cost and toxicity, as well as chemical and thermal stability [16].

In contrast to adsorption and absorption-based concepts, membrane and condensation-based separations enable continuous operation without dedicated working fluids or cyclic regeneration steps. Moreover, both condensation and membrane separation can be implemented as standalone unit operations and combined with reaction steps. This allows for straightforward process design based on in principle well-known technologies. The present work therefore places the focus on these two separation principles.

1.1. Condensation

Condensation is the state-of-the-art method for product separation from the methanol loop [17]. Apart from the standard single-stage reactor with one condensator after the reactor, process concepts with condensation separation between typically two reaction stages can be found in commercial large-scale configurations, e.g., in the Johnson Matthey/Davy Process Technology "Original Series Loop" [18] and in the Nextchem/GasConTec/Thyssenkrupp "AdWinMethanol" process concept [19]. Multi-stage concepts for conventional methanol synthesis with more than two alternating reaction and separation units have also been proposed in the patent literature by major technology owners e.g., Thyssenkrupp [20], Mitsubishi [21], Johnson Matthey [22], and Air Liquide [23]. These concepts differ in design aspects, such as the types of reactors employed, the placement of recycle compressors, and the overall flow configuration (e.g., bypasses, feed distribution). For synthesis gas with inert contents too high to recycle, cascaded once-through configurations have been suggested as an alternative [24–26].

In light of the specific challenges associated with CO_2-based methanol synthesis, there has been renewed interest in interstage condensation-based process configurations. Lacerda de Oliveira Campos et al. [7] performed a techno-economical analysis of a serial reactor module (three stages) configuration at an operating pressure of 70 bar with intermediate condensation steps. Compared to a parallel reactor module arrangement, they reported that the benefits of a reduced recycle flow, such as smaller equipment sizes and less reactant loss in the purge stream, outweigh the cost incurred by the additional heat exchange and separation equipment. In the context of small-scale renewable energy storage, Moioli et al. [27] compared different CO_2-based methanol synthesis process configurations at an operating pressure of 50 bar including a single-pass reactor, a recycle reactor, and a cascaded reactor arrangement without recycle. They argued that for small-scale operation with energy scarcity, the cascaded reactor configuration is best suitable due to its lower energy requirement and high methanol yield. In a follow-up work, Moioli et al. [28] investigated the techno-economical feasibility of several small-scale, multistage process configurations at an operating pressure of 30 bar, differing in the type of valorization of unconverted reactants (recycling vs. coupling with methanation) and CO_2 source (pure vs. biogas). The recycle process from pure CO_2 and the cascade from biogas including subsequent methanation were shown to perform economically similar and tolerate the highest electricity cost. Hillestad [29] investigated several interstage condensation concepts from CO_2 at an operating pressure of 82 bar. The study compared a once-through configuration, where hydrogen was recovered from the unconverted reactants in a pressure swing adsorption unit, with a recycle configuration, in which unconverted reactants were returned directly to the reactor without separation. The optimal catalyst volume distribution, coolant temperature and hydrogen feed distribution was found by maximizing the per-pass methanol production while using the least possible reaction volume and hydrogen. A three-stage configuration with recycle was claimed the best compromise and a final design is proposed with the reaction stages located in a common shell, closely resembling a patent by Gal et al. [30]. Patent filings from major technology licensors further illustrate the industrial interest in interstage condensation for CO_2-based methanol synthesis: AirLiquide report their latest "Generation 2.1" CO_2-based methanol process concept to be a three-stage configuration with each stage containing water-cooled reactor, heat exchangers and separator in a common vessel [31,32]. In another patent, they propose a multi-stage condensation scheme in which the recycle stream is sufficiently reduced to be integrated directly with the feed compressor train [33]. Thyssenkrupp describe a two-stage reactor configuration with interstage condensation [34], and Topsøe propose a two-stage arrangement combining interstage condensation with a shared boiling water shell [35].

1.2. Membranes

In methanol synthesis, membrane separation is primarily investigated for the selective removal of MeOH and/or H_2O through a membrane to maintain distance from chemical equilibrium, while unconverted reactants H_2, CO_2, and CO are retained. Pioneering work on membranes in methanol synthesis began in the 1990s with Struis et al. [36] being the first to experimentally demonstrate the feasibility of in-situ product separation via membrane technology. Since then, a research field has emerged which can be categorized into three key areas: the development of suitable membrane materials, reaction engineering utilizing these membranes, and process engineering focused on embedding membrane-based reaction/separation technologies. Up to now, product separation using membranes is not state-of-the-art in methanol synthesis.

Membrane materials used in methanol synthesis can be divided into polymers, zeolites and carbon membranes. Fig. 1 gives an overview of reported permeance and selectivity data of these membrane types for H_2O and MeOH, respectively. Most membranes used in conventional applications today are fabricated from polymers, owing to their relatively low production costs, ease of scalability [37], and the availability of processing techniques for consistently producing thin membrane structures [38]. Struis et al. [36] used a polymeric cation-exchange membrane (Nafion^{TM}) for their early experiments. The material, however, showed decomposition above 200 °C, which is below the operating temperature of the conventional Cu-based methanol synthesis catalyst. This has motivated the investigation of more temperature-resistant polymeric materials, such as polyimides (PI) [39], polybenzimidazole (PBI) [40], and sulfonated poly ether ether ketones (SPEEK) [41,42], and composite materials, such as silicon on ceramic support [43,44]. Although H_2O and MeOH permeance remain relatively high for these membranes at temperatures exceeding 200 °C (Fig. 1(a) and Fig. 1(c)), the selectivity towards H_2 decreases drastically (Fig. 1(b) and Fig. 1(d)). Zeolites represent another widely studied class of membrane materials in the context of methanol synthesis, primarily due to their superior thermal stability, which aligns better with the operating conditions of conventional methanol synthesis processes [45]. Moreover, even at temperatures above 200 °C, they tend to provide higher product permeability at high selectivity towards H_2 than polymer membranes (Fig. 1). Investigated zeolite types are various and include, among others, FAU-type [46], MOR-type [47], Type A (LTA) [48,49], and promising Type

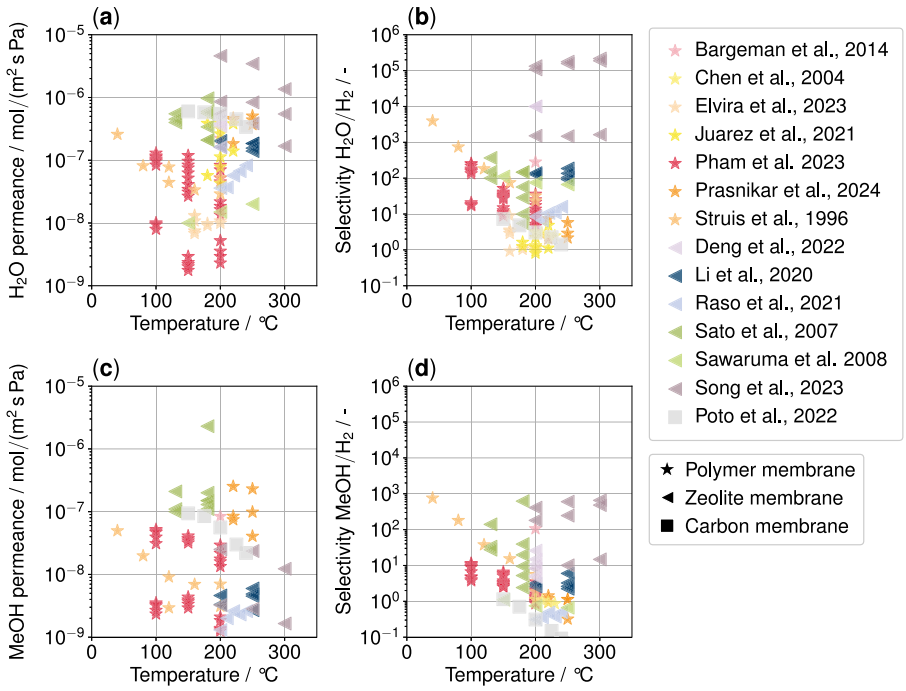

Fig. 1. Temperature-dependent (a) H_2O permeances, (b) H_2O/H_2 selectivities, (c) MeOH permeances, and (d) $MeOH/H_2$ selectivities of selected membranes reported in literature for methanol synthesis. Polymeric membranes: Struis et al. [36],Pham et al. [39],Elvira et al. [40],Prašnikar et al. [41],Bargeman et al. [42],Chen and Yuan [43],Juarez et al. [44]. Zeolite membranes: Sato et al. [46],Sawamura et al. [47],Song et al. [48],Raso et al. [49],Li et al. [50],Deng et al. [51]. Carbon membranes: Poto et al. [53].

Na-A (LTA) [50,51]. However, the defect-free and reproducible fabrication of zeolite membranes remains a significant challenge, posing a major obstacle to large-scale production [38,52]. Carbon membranes as molecular sieves have been investigated in methanol synthesis as well [53]. Although promising in terms of cost and ease of preparation, they are less commonly reported in the literature [52].

Studies on methanol synthesis employing membranes for product separation, both at reaction and process engineering level, are mostly focused on membrane reactors, i.e., the integration of reaction and separation functionality in a single unit. Different membrane reactor configurations are summarized in a recent review by Richard et al. [54]. From a reaction engineering level, there is broad scientific consensus emphasizing the superior performance of membrane reactors over conventional tubular reactors in terms of single-pass reactant conversion and methanol yield [45,49,55–57]. Although in principle suggested early by Struis and Stucki [58], to the best of our knowledge, Sjöberg et al. [59] were the only ones to investigate interstage product separation by membranes in the context of methanol synthesis, assuming a CO-rich synthesis gas from black liquor gasification. Using experimental permeation data for zeolite ZSM-5 membranes, they compared the performance of a conventional reactor with recycle, a single-pass membrane reactor and a single-pass membrane-module reactor on a reaction engineering level. Single-pass conversion increased from 26 % in the conventional reactor to 97 % in the membrane reactor and 81 % in the membrane-module reactor, while the required amount of catalyst in the latter two almost halved due to the omission of the recycle. Permeation data was, however, strongly extrapolated from ambient temperature and atmospheric pressure to the reaction conditions of a conventional Cu-based catalyst, questioning the reliability of the superior performance of the membrane-based processes.

On a process engineering level, studies are generally fewer in number and tend to reach more cautious conclusions, particularly regarding the impact of H_2 co-permeation on process/system performance metrics. To quantify this aspect, Hamedi et al. [60] assessed the thermodynamic performance of a CO_2-based methanol process employing a 1D membrane reactor model at 50 bar to 70 bar synthesis pressure on the retentate side and atmospheric pressure on the permeate side. Assuming an idealized, infinitely selective zeolite membrane and a constant H_2O permeance of 1×10^{-6} mol m^{-2} s^{-1} Pa^{-1}, their analysis demonstrated that, under these ideal conditions, the membrane-based process could reduce power consumption by 32 % and increase exergy production by 21 % compared to the conventional process. Based on a target-based approach where both the membrane-based and the conventional process achieve the same power consumption and exergy production, the required H_2O/H_2 selectivity was determined to be 970 and 190, respectively. In a similar target-based study, Dieterich et al. [61] conducted a techno-economic assessment of a CO_2-based methanol process using a membrane reactor at 70 bar synthesis pressure. Their process layout also considered a 1D membrane reactor model, but differed by incorporating an additional H_2 sweep on the permeate side of the reactor. When comparing two process configurations with different sweep pressures (same pressure as make-up feed and atmospheric), they found that only the atmospheric sweep had an economic advantage over the conventional process. For this layout, H_2 co-permeation was found to be a critical parameter for sufficient MeOH yield and a minimum H_2 permeance of 1×10^{-9} mol m^{-2} s^{-1} Pa^{-1} was specified. The maximum allowable membrane costs derived from the economic comparison with the conventional process were shown to mainly depend on H_2O permeance, and a target of 5×10^{-7} mol m^{-2} s^{-1} Pa^{-1} was recommended.

Both studies on the process engineering level state, that process intensification in terms of the integrated membrane reactor increases the complexity of the process and poses further implicit challenges for material development. For example, Dieterich et al. [61] emphasize that membrane development needs to focus on pressure stability in order to withstand pressure differences of 50 bar to 100 bar when using conventional Cu-based catalysts. Moreover, they report that the targeted high H_2O permeance also leads to increasing hotspot temperatures on the retentate side of the membrane reactor, which may pose additional challenges to catalyst and membrane stability. This was particularly crucial, as the membrane lifetime (and thus the frequency of its replacement) had a major impact on economic performance in comparison to the conventional process. Hamedi et al. [60] conclude

that their results for the required H_2O/H_2 selectivities must be understood only as lower threshold values due to the increased system complexity.

1.3. Scope of this work

An interstage arrangement of product separation units is able to exploit the advantage of product removal on the equilibrium-limitation while avoiding the aforementioned inherent drawbacks of in-situ intensified units related to the reduction in degrees of freedom and engineering complexity. For the membrane separation unit, this strategy decouples the membrane conditions from the reaction conditions and allows to control the temperature of each unit individually, which would particularly enable the use of low-cost and mass-produced polymer membranes. The condensation separation unit is already based on commercially proven and available technology, however likely associated with a larger heat transfer intensity due to repeated heating and cooling.

In this work, we investigate the impact of two interstage product separation strategies on the performance of the CO_2-based methanol synthesis process. Condensation and membrane units are considered as separation technologies, with a single-stage condensation process serving as the reference case. The process configurations are evaluated from a process engineering perspective, taking into account the entire synthesis section from H_2 and CO_2 feed to crude methanol to assess how the different separation strategies influence key performance metrics. This study thus contributes to the development of CO_2-based methanol processes through the following novelties:

- Process-wide simulation of interstage product separation strategies, capturing trade-offs beyond reactor performance.
- Comparison of interstage condensation and membrane separation as competing intensification strategies.
- Identification of operating regimes for interstage membrane separation using polymer membranes.

2. Methods

2.1. Process concepts

The flowsheets of the different process concepts investigated in this study are shown in Fig. 2. The single-stage recycle loop is considered as a reference (*reference process*). The concept of interstage condensation (*condensation process*) is adopted from Haag et al. [31]. The corresponding configuration using interstage membrane units (*membrane process*) has not been considered in the literature to the best of our knowledge. All processes are modeled in AVEVA™ Process Simulation 2024.1 [62] using the Soave-Redlich-Kwong equation of state [63] as the underlying thermodynamic model.

The CO_2 make-up feed (stream ① in Fig. 2) is assumed to be available at 25 °C and 1.013 bar, with a purity of $y_{CO_2,①} = 98\,\%$ [64]. To consider the accumulation of inerts in the process, the rest is assumed to be N_2 ($y_{N_2,①} = 2\,\%$), similar to the assumptions by Lacerda de Oliveira Campos et al. [7]. The H_2 make-up feed (stream ② in Fig. 2) is introduced at 25 °C and 30 bar [7]. It is assumed to be supplied by electrolysis meeting Type I Grade C specifications ($y_{H_2,②} = 99.999\,\%$, $y_{H_2O,②} = 0.0009\,\%$, $y_{O_2,②} = 0.0001\,\%$) [65]. The overall make-up feed (streams ① + ②) is characterized by a stoichiometric number of $SN = 2.05$, as defined in Eq. (1), and an overall molar flow of $\dot{N}_{①+②} = 700\,\mathrm{kmol\,h^{-1}}$. From reaction stoichiometry, this corresponds to a methanol plant with a maximum methanol production of $132\,\mathrm{t\,d^{-1}}$.

$$SN = \frac{y_{H_2} - y_{CO_2}}{y_{CO} + y_{CO_2}} \tag{1}$$

The purge fraction ξ_{Purge}, resulting in the purge stream ③, is set to a constant value of 2 % of the unconverted gas leaving the last separation stage [7].

In both the reference and condensation processes, both make-up feeds ① and ② are compressed independently to the process pressure $p_{Process}$, mixed with the recycle stream, and subsequently fed into the reactor. Unconverted reactants are re-compressed to $p_{Process}$, and recycled back to the first reactor. In the membrane process, reactants that co-permeate through the membrane must also be recycled to avoid unrecoverable losses, which would otherwise compromise the viability of the process. Given the high partial pressure of H_2 present in both the reactors and on the retentate side of the membranes, H_2 permeation is expected to be particularly critical. To suppress H_2 permeation to the permeate side, thereby minimizing its energy-intensive re-compression required for its recovery, a H_2-rich sweep gas can be used. This is effectively accomplished by choosing the H_2 make-up feed ② itself as the sweep gas. Thus, the H_2 make-up feed ② is first compressed to the pressure p_{Sweep} and fed into a sweep cycle. After final separation of the condensable components, a fraction ξ_{StP} (sweep-to-process) of the hydrogen-rich sweep gas is compressed to the process pressure $p_{Process}$, mixed with the CO_2 make-up feed ① and introduced into the first reactor stage. The remaining sweep gas is re-compressed to p_{Sweep} and recycled back to the sweep cycle inlet, where it is mixed with the H_2 make-up feed ②. The CO_2 make-up feed ① is directly compressed to $p_{Process}$.

In the condensation and membrane processes, the concept of interstage product removal is realized by an alternating arrangement of reaction units and separation units (separator drum or membrane). The entity of heater, reaction unit, cooler and separation unit is referred to as *reaction-separation stage*, as highlighted in Fig. 2. The number of reaction-separation stages in series is denoted by N. Finally, the crude methanol stream ④ is obtained.

2.2. Unit models

Reaction units. The reaction units are assumed as tubular water-cooled reactors and are modeled as equilibrium reactors, considering the two exothermic methanol synthesis reactions in Eqs. (R1) and (R2) and the endothermic reverse water-gas shift reaction in Eq. (R3).

$$CO_2 + 3\,H_2 \rightleftharpoons CH_3OH + H_2O \qquad \Delta\bar{H}_R^0 = -49.4\,\mathrm{kJ/mol} \tag{R1}$$

$$CO + 2\,H_2 \rightleftharpoons CH_3OH \qquad \Delta\bar{H}_R^0 = -90.7\,\mathrm{kJ/mol} \tag{R2}$$

$$CO_2 + H_2 \rightleftharpoons CO + H_2O \qquad \Delta\bar{H}_R^0 = 41.2\,\mathrm{kJ/mol} \tag{R3}$$

Equilibrium constants are adopted from Graaf and Winkelman [66] and implemented according to the following equations:

$$K_f = \prod_{i=1}^{K} \left(\frac{f_i(T,p,y_j)}{p^0} \right)^{\nu_i} \tag{2}$$

$$\ln K_f^{(R2)} = \frac{1}{\bar{R}T} \left(a_1 + a_2 T + a_3 T^2 + a_4 T^3 + a_5 T^4 + a_6 T^5 + a_7 T \ln T \right) \tag{3}$$

$$\ln K_f^{(R3)} = \frac{1}{\bar{R}T} \left(b_1 + b_2 T + b_3 T^2 + b_4 T^3 + b_5 T^4 + b_6 T^5 + b_7 T \ln T \right) \tag{4}$$

$$K_f^{(R1)} = K_f^{(R2)} \cdot K_f^{(R3)} \tag{5}$$

Therein, K_f is the equilibrium constant of each reaction calculated for ideal gases at temperature T. Non-idealities are contained in the fugacities $f_i(T,p,y_j)$ for each considered species i and are calculated from the equation of state. The stoichiometric coefficients are denoted by ν_i. The polynomial parameters a_{1-7} in Eq. (3) and b_{1-7} for Eq. (4) are provided Table 1.

The inlet temperature $T^{(n)}_{Reactor,in} = 230\,°C$ and outlet temperature $T^{(n)}_{Reactor,out} = 250\,°C$. These temperature values are chosen to be in the range of pilot and demo plants for CO_2-based methanol processes reported by Dieterich et al. [4] and are considered the same for every reaction stage (n) in each of the processes. The reverse water-gas shift

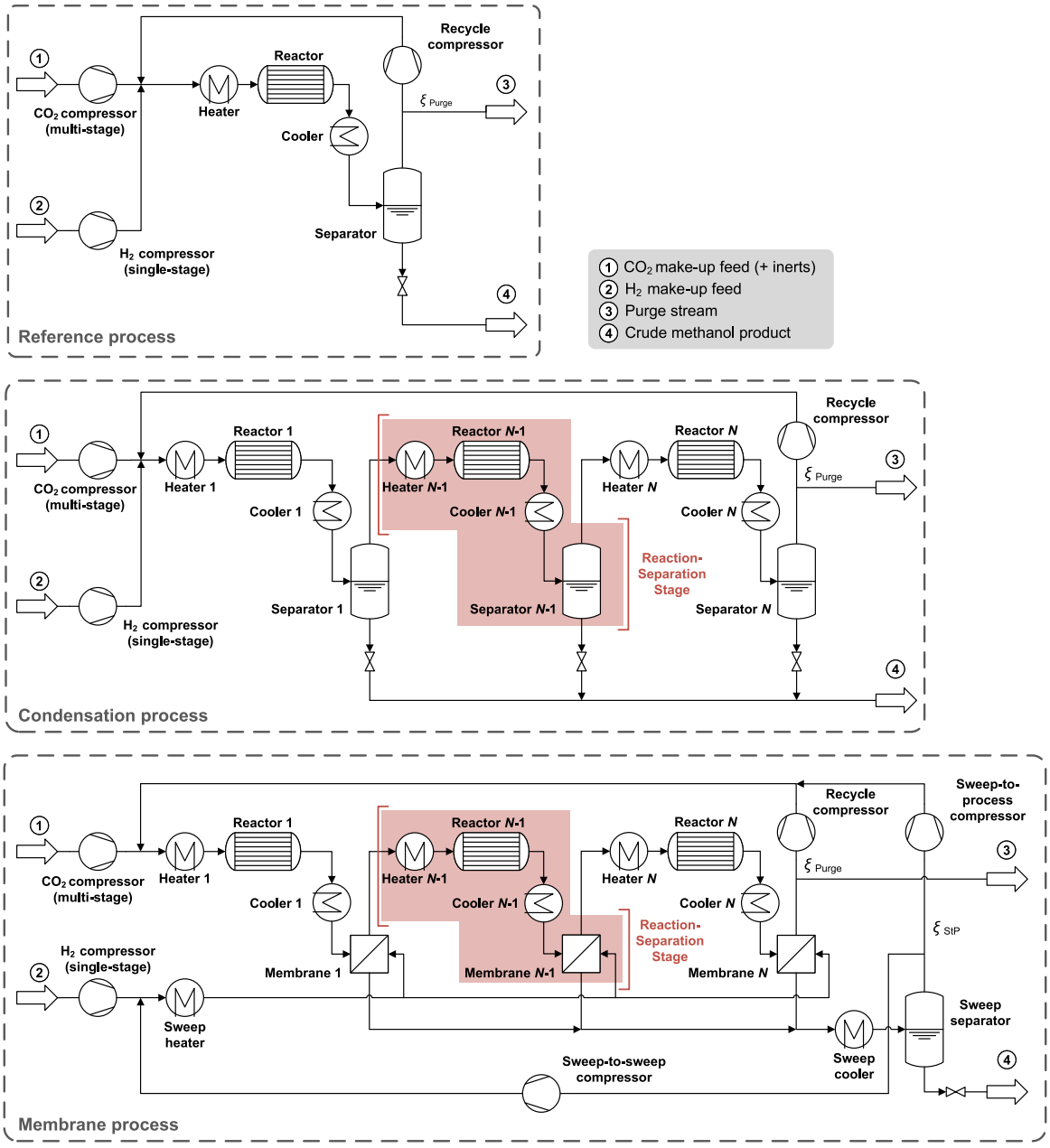

Fig. 2. Flowsheets of the reference, condensation, and membrane process layouts.

Table 1
Polynomial parameters of equilibrium constants [66].

Parameter i	Eq. (R2) (a_i)	Eq. (R3) (b_i)
1	$7.44140 \cdot 10^{4}$	$-3.94121 \cdot 10^{4}$
2	$1.89260 \cdot 10^{2}$	$-5.41516 \cdot 10^{1}$
3	$3.2443 \cdot 10^{-2}$	$-5.5642 \cdot 10^{-2}$
4	$7.0432 \cdot 10^{-6}$	$2.5760 \cdot 10^{-5}$
5	$-5.6053 \cdot 10^{-9}$	$-7.6594 \cdot 10^{-9}$
6	$1.0344 \cdot 10^{-12}$	$1.0161 \cdot 10^{-12}$
7	$-6.4364 \cdot 10^{1}$	$1.8429 \cdot 10^{1}$

reaction in Eq. (R3) is assumed to reach equilibrium conditions. This assumption is based on its faster kinetics compared to the CO_2-based synthesis reaction in Eq. (R1) [67]. The latter is modeled with an approach-to-equilibrium (ATE) of 20 K [68] for each reaction stage, acknowledging that full chemical equilibration is not reached in practice while avoiding explicit reactor sizing at each parameter variation. A comparison of this ATE method to reaction kinetics from Nestler et al. [69] and Graaf et al. [70] is provided in the supplementary information (SI). The pressure drop of the reaction unit in the reference process is assumed to be $\Delta p_{\mathrm{Reactor}} = 3\,\mathrm{bar}$, similar to a conventional medium-scale, tubular water-cooled reactor [4,71]. This value is assumed to be equally distributed among the N reaction units for the condensation and membrane processes, to consider the fact that product removal reduces the throughput and reactor size in each subsequent stage.

Heater/cooler units. Heating and cooling of the process and sweep streams is modeled by standard, built-in heater/cooler units. The pressure drop of each heater/cooler unit in each of the processes is assumed to be $\Delta p_{\mathrm{HCU}} = 0.2\,\mathrm{bar}$ [72].

Membrane units. The membrane units are modeled as 1D counter-current membrane modules using the built-in shortcut model in AVEVA Process Simulation. This shortcut model originates from Bishop and Lima [73], where the model was verified against data from Radcliffe

et al. [74]. The reactor outlet is passed to the retentate side of the membrane, and the permeate is withdrawn using the sweep.

The differential material balances for retentate and permeate side are given in Eqs. (6) and (7), respectively.

$$\frac{d\dot{N}_{i,r}}{dA} = -J_i \tag{6}$$

$$\frac{d\dot{N}_{i,p}}{dA} = J_i \tag{7}$$

Therein, the change in molar flow $\dot{N}_i$ of each species i along the membrane area A, is determined by the trans-membrane flux J_i of each species i. The subscripts r and p denote retentate and permeate side, respectively. The differential energy balances for retentate and permeate side are given in Eqs. (8) and (9), respectively.

$$\frac{d\dot{H}_r}{dA} = -\left(U_{\text{mem}}(T_r - T_p) + \sum_i J_i\left(\bar{H}_{i,r} - \bar{H}_{i,p}\right)\right) \tag{8}$$

$$\frac{d\dot{H}_p}{dA} = \left(U_{\text{mem}}(T_r - T_p) + \sum_i J_i\left(\bar{H}_{i,r} - \bar{H}_{i,p}\right)\right) \tag{9}$$

Therein, the change in enthalpy flow $\dot{H}$ of each stream along the membrane area A is determined by a term for convective heat transfer, using an overall heat transfer coefficient $U_{\text{mem}} = 30\,\text{W}\,\text{m}^{-2}\,\text{K}^{-1}$ as a typical value for gas-to-gas heat transfer [75], and the trans-membrane enthalpy flux dependent on the molar enthalpy $\bar{H}$ of each permeated species i.

Both, retentate and permeate side are discretized into 20 sections. The outlet condition of each section determines the thermodynamic state within each section of the respective side, thus transforming the differential equations into algebraic equations.

Following the model by Bishop and Lima [73], the trans-membrane flux J_i is calculated from the linear relationship in Eq. (10) from the difference in partial pressures p_i between retentate and permeate side, and a membrane-specific permeance P_i for each species i.

$$J_i = P_i\,(p_{i,r} - p_{i,p}) \tag{10}$$

The interstage-arrangement of membranes aims to enable the use of inexpensive and mass-producible polymer membranes by setting the operating temperature of the membrane module independently of the reaction conditions, i.e., at lower temperatures. An inlet temperature of 200 °C is assumed on both sides of the membrane, selected as a balance between minimizing the repeated cooling and heating required between reaction and separation stages on the one hand, and remaining within the thermal limits of polymeric membrane materials on the other hand. While this value is reported as the upper decomposition threshold for Nafion™ as membrane material [36,44], temperature-resistant polymeric materials [39–42] are reported at or beyond this temperature (see Fig. 1).

Permeability measurement conditions for membranes often differ significantly from the intended application conditions, particularly in feed composition (pure or mixed) or membrane thickness [38]. The data sources underlying Fig. 1 differ in feed composition (partial pressure values of H_2O and MeOH, single-component vs. mixture), absolute retentate and permeate pressures, operating temperature, membrane thickness, and membrane geometry. Selecting any one dataset would therefore require uncertain extrapolation to the conditions of interest, as required when exploring different designs and operating conditions in this study. To cope with this uncertainty, we assume a hypothetical polymer membrane with constant permeances, treating membrane permeances as free parameters, as done in similar process-based studies [60,61]. The sensitivity of the results to these permeance/selectivity parameters is assessed in Section 2.3. Given the typically desired high permeability of products (H_2O, MeOH) and high selectivity over reactants (H_2, CO_2), these values are placed in the upper range of values reported in the literature at the chosen membrane temperature of 200 °C (Fig. 1). Based on the recommendation by Dieterich et al. [61], we assume a H_2O permeance value of $P_{H_2O} = 5 \times 10^{-7}\,\text{mol}\,\text{m}^{-2}\,\text{s}^{-1}\,\text{Pa}^{-1}$. As shown in Fig. 1(a), this is an optimistic but potentially feasible estimate for polymer membranes. The assumed selectivities of the considered species in relation to water are given in Table 2. The influence of selectivities of H_2 and MeOH in relation to H_2O is discussed in Section 2.3. Since permeation data for CO and N_2 in the context of methanol synthesis is largely unavailable for the polymer membranes shown in Fig. 1, permeances of CO and N_2 are assumed to be significantly lower than that of CO_2 and therefore considered negligible. This assumption is supported by literature reporting generally positive CO_2/CO [73,76] and CO_2/N_2 selectivities [73,77] for various polymer membranes, albeit in different applications.

Table 2
Assumed selectivities for each species i in relation to H_2O ($P_{H_2O} = 5 \times 10^{-7}\,\text{mol}\,\text{m}^{-2}\,\text{s}^{-1}\,\text{Pa}^{-1}$).

Species i	Selectivity P_{H_2O}/P_i
MeOH	10
H_2	100
CO_2	1000

In the absence of detailed specifications for the geometry of the membrane module, an initial membrane area of $A^{(n)} = 6000\,\text{m}^2$ per module n is assumed. Similarly, pressure drops on retentate $\Delta p_{r,\text{Membrane}}$ and permeate side $\Delta p_{p,\text{Membrane}}$ depend on the membrane module type, geometry and structure. Therefore, we take $\Delta p_{r,\text{Membrane}} = \Delta p_{p,\text{Membrane}} = 0.5\,\text{bar}$ as an assumption. These parameters serve as a basis for initial analysis and will be investigated to assess their influence on the process, see Section 2.3.

Separator units. The separator temperature is uniformly set to $T_{\text{Separator}} = 40\,°\text{C}$ for all process configurations, achievable with conventional cooling water recooled in a cooling tower [78]. To ensure that differences in process performance can be attributed solely to the separation characteristics of the two investigated separation strategies, a consistent pressure drop of $\Delta p_{\text{Separator}} = \Delta p_{r,\text{Membrane}} = \Delta p_{p,\text{Membrane}} = 0.5\,\text{bar}$ is applied to all separators within the reaction-separation unit. The sweep separator in the membrane process is considered without pressure drop. For the reference process, this results in an overall pressure drop of 3.9 bar in the loop, which is within the range of conventional loops based on a tubular, water-cooled reactor as reported by Dieterich et al. [4].

Compressors. Each compressor is considered with a constant isentropic efficiency of $\eta_{\text{is}} = 75\,\%$ [79]. For each process, compression of the CO_2 make-up feed ① is assumed in five stages with intercooling to 40 °C and a constant pressure ratio calculated by Eq. (11) [80]. The H_2 make-up feed ② is compressed in a single stage.

$$\Pi = \left(\frac{p_{\text{Process}}}{1.013\,\text{bar}}\right)^{1/5} \tag{11}$$

2.3. Case studies

To systematically compare the condensation and membrane-based process concepts (Fig. 2), a range of key process parameters is explored, with a consistent simulation framework applied across all scenarios. The process pressure p_{Process} is varied within the range reported by Dieterich et al. [4] for pilot and demo plants. Further, the number of reaction-separation stages N for both process concepts, and membrane-specific parameters such as sweep pressure p_{Sweep} and sweep-to-process split ξ_{StP}, membrane stage area $A^{(n)}$ and pressure drops $\Delta p_{p,r}^{(n)}$, as well as H_2O/H_2 and H_2O/MeOH selectivities are investigated. A base case is defined to establish a point of reference for evaluation. The set of parameter ranges and assumptions is listed in Table 3.

Table 3
Summary of base case values and parameter ranges used for process concept comparison. Base case values are underlined.

Parameter	Symbol	Range/Value	Ref.	Cond.	Memb.
Varied in Section 3.1 and Section 3.2					
Process pressure	p_{Process}	40 bar to 100 bar	✓	✓	✓
Sweep pressure	p_{Sweep}	20 bar to p_{Process}			✓
Sweep-to-process split	ξ_{StP}	0.01 to 0.20			✓
Fixed in Section 3.1, varied in Section 3.2					
Number of stages	N	2, 3, 5		✓	✓
Membrane area	$A^{(n)}$	2000, 4000, 6000, 10 000 m^2			✓
Membrane pressure drop	$\Delta p_{p,r}^{(n)}$	0, 0.5 bar			✓
Membrane selectivity	$P_{\text{H}_2\text{O}}/P_{\text{H}_2}$	10, 100, 1000			✓
Membrane selectivity	$P_{\text{H}_2\text{O}}/P_{\text{MeOH}}$	1, 10, 50			✓

2.4. Performance indicators

The key performance indicators used to evaluate and compare the process concepts are carbon efficiency η_C (Eq. (12)), total specific compressor power $e_{\text{comp,total}}$ (Eq. (13)), and total specific heat transfer q_{total} (Eq. (14)). The carbon efficiency η_C indicates how effectively the carbon contained in the CO_2 feedstock is converted into MeOH. It is defined as the ratio of MeOH molar flow rate in the crude methanol stream ④, $\dot{N}_{④,\text{MeOH}}$, to the constant CO_2 molar flow rate in the CO_2 make-up feed ①, $\dot{N}_{①,\text{CO}_2}$. The total specific compressor power $e_{\text{comp,total}}$ reflects the combined electric load of all compressors and serves as a proxy for the size and energy intensity of the rotating equipment in relation to $\dot{N}_{①,\text{CO}_2}$. The total specific heat transfer q_{total}, defined as the sum of absolute heating and cooling demands in relation to $\dot{N}_{①,\text{CO}_2}$, indicates the overall thermal load and is used as a measure for the required size of the heat exchangers.

$$\eta_C = \frac{\dot{N}_{④,\text{MeOH}}}{\dot{N}_{①,\text{CO}_2}} \tag{12}$$

$$e_{\text{comp,total}} = \frac{\sum_i P_{\text{el,comp},i}}{\dot{N}_{①,\text{CO}_2}} \tag{13}$$

$$q_{\text{total}} = \frac{\sum_i |\dot{Q}_i|}{\dot{N}_{①,\text{CO}_2}} \tag{14}$$

3. Results

3.1. Base case

The base case at a constant number of reaction-separation stages and constant membrane parameters (see Table 3) serves as reference for the following parameter variations.

3.1.1. General results

Systematic variation of the process pressure p_{Process}, sweep pressure p_{Sweep} and sweep-to-process split ξ_{StP} within the ranges specified in Table 3 yields the curves (reference and condensation process) and point clusters (membrane process) depicted in Fig. 3. For the membrane process, a dashed line indicates the convex hull of each cluster. The highlighted design points on the Pareto-like fronts have the minimum relative distance to the condensation process in Fig. 3 at the same process pressure p_{Process}. The corresponding parameters and results, along with those of the reference and condensation processes, are listed in Table 4.

For the single-stage reference process, carbon efficiency η_C increases with process pressure p_{Process} due to higher conversion from a more favorable equilibrium, thereby reducing loop flow and associated purge losses. Below 60 bar, the power demand remains approximately constant. Above, it increases, as the additional compression required for the feed begins to outweigh the reductions in recycle compression from improved conversion. The condensation process achieves higher carbon efficiencies than the reference process by leveraging interstage product

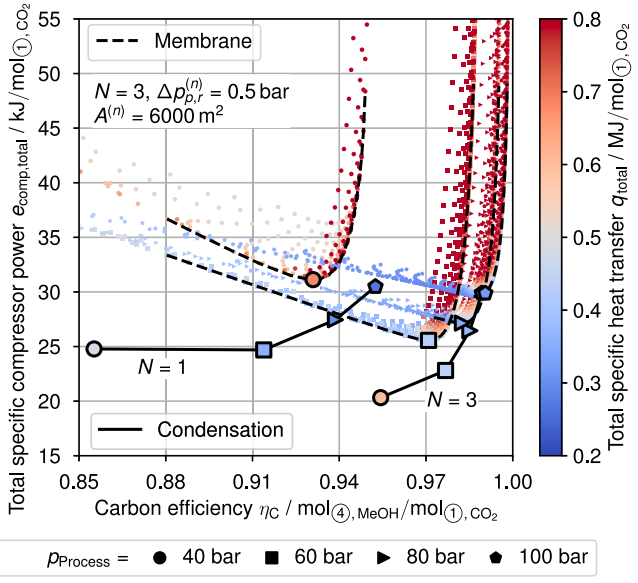

Fig. 3. Comparison of the reference ($N = 1$), condensation ($N = 3$), and membrane process ($N = 3$) for different process pressures p_{Process}. Each point in the clusters of the membrane process represents a different design resulting from variation of the sweep pressure p_{Sweep} and sweep-to-process split ξ_{StP}. Highlighted design points on trade-off curves have minimum distance to condensation design point at the same p_{Process}. Other parameters correspond to the base case values in Table 3.

removal, enhancing conversion and reducing carbon losses via the purge. This improvement is, however, offset by the increased demand in overall heat transfer, indicated by the total specific heat transfer q_{total}, due to the repeated cooling and heating, being particularly evident at lower process pressures. As the process pressure increases, conversion improves further, lowering loop flow and reducing heat transfer requirements at the cost of higher feed compression energy. For the 3-stage condensation process, the process pressure range of 60 bar to 80 bar emerges as a reasonable compromise, offering significantly improved carbon efficiency with heat transfer requirements in the same order of magnitude as the reference process. Pinch analysis of the interstage condensation design cases in Table 4 shows that, within the considered system boundary, the external energy requirement does not change significantly compared to the reference case (see SI).

For the membrane process, the relationship between total specific compressor power and carbon efficiency is characterized by convex trade-off curves (indicated by dashed lines in Fig. 3) for each process pressure p_{Process}, forming Pareto-like fronts around the respective point clusters. At low process pressures p_{Process}, the membrane process achieves higher carbon efficiency than the reference process, albeit with substantially increased energy consumption and heat transfer requirements. Its performance remains clearly inferior to that of the

Table 4
Highlighted design cases in Fig. 3 for reference (R), condensation (C), and membrane (M) process.

$p_{Process}$/bar	40			60			80			100		
	R	C	M	R	C	M	R	C	M	R	C	M
N/-	1	3	3	1	3	3	1	3	3	1	3	3
p_{Sweep}/bar	–	–	32	–	–	49	–	–	65	–	–	76
ξ_{StP}/-	–	–	0.05	–	–	0.08	–	–	0.10	–	–	0.14
$\dot{N}_{③}$/kmol h^{-1}	104	40	54	67	26	30	51	20	22	41	18	17
$\dot{N}_{④}$/kmol h^{-1}	301	331	324	318	338	336	326	341	339	331	342	342
$y_{④,H_2O}$/%	50.7	50.2	50.6	50.1	49.9	50.1	49.9	49.9	50.0	49.8	49.8	49.9
$y_{④,MeOH}$/%	48.9	49.5	49.3	49.4	49.7	49.7	49.5	49.7	49.8	49.5	49.8	49.9
η_C/%	85.5	95.4	93.0	91.4	97.7	97.0	93.9	98.5	98.3	95.3	98.9	99.1
$e_{comp,total}$/ $\frac{kJ}{mol_{①,CO_2}}$	24.8	20.3	31.2	24.7	22.8	25.6	27.5	26.5	27.1	30.5	29.9	29.9
$\frac{kJ}{mol_{④,MeOH}}$	29.0	21.3	33.5	27.0	23.3	26.4	29.3	26.9	27.6	32.0	30.2	30.2
q_{total}/ $\frac{MJ}{mol_{①,CO_2}}$	0.48	0.59	0.66	0.35	0.43	0.42	0.29	0.37	0.34	0.25	0.33	0.32
$\frac{MJ}{mol_{④,MeOH}}$	0.56	0.62	0.71	0.38	0.44	0.43	0.31	0.38	0.35	0.26	0.33	0.32

condensation process. At lower process pressures $p_{Process}$, the equilibria of the synthesis reactions Eqs. (R1) and (R2) shift less toward the products, resulting in lower product partial pressures on the retentate side of the membranes. Because the product partial pressures in the lean sweep feed are fixed by the sweep condenser temperature, the driving force for separation in Eq. (10) remains small. Consequently, the membrane area limits overall product separation. Owing to the lower permeability of MeOH compared to H_2O (see Table 2), MeOH accumulates in the recycle loop, leading to an increased recycle demand and to carbon loss via the purge. The effect of membrane area and MeOH permeance on process performance is further analyzed in Section 3.2.2. As the process pressure $p_{Process}$ increases, the membrane process curves approach the performance of the condensation process.

The molar fractions of H_2O and MeOH in the crude methanol stream ④ are given in Table 4 for all configurations and process pressures. The molar ratio of H_2O to MeOH is close to 1 in all cases, consistent with the global reaction stoichiometry. Deviations can be attributed to the differences in vapor pressure of methanol and H_2O and gas solubilities across the pressure ranges investigated ($p_{Process}$ and p_{Sweep}).

3.1.2. Detailed results

To better analyze the characteristics of the membrane process, several design cases are examined in detail. These selected design cases are summarized in Table 5. A process pressure of $p_{Process} = 80\,bar$ is chosen as the basis for the analysis. Membrane cases A-C vary the sweep pressure p_{Sweep} at constant sweep-to-process split ξ_{StP}, while D-F vary ξ_{StP} at fixed p_{Sweep}. Note that B and E describe the same design point. In addition to the overall carbon efficiency η_C, the single-pass CO_2 conversion $X_{CO_2,SP}$ as a reactor-level indicator is calculated using Eq. (15) and given in Table 5.

$$X_{CO_2,SP} = \frac{\sum_{n=1}^{N} X_{CO_2}^{(n)}\, \dot{N}_{CO_2,Reactor,in}^{(n)}}{\dot{N}_{CO_2,Reactor,in}^{(1)}} \tag{15}$$

For $N = 3$, interstage condensation increases the single-pass conversion $X_{CO_2,SP}$ by a factor of ca. 2.5 compared to the single-stage reference process. In contrast, the single-pass conversion $X_{CO_2,SP}$ in the membrane process is highly sensitive to the design parameters $p_{Process}$ and ξ_{StP}.

To analyze the membrane-level transport processes and their dependence on the design parameters p_{Sweep} and ξ_{StP}, Fig. 4 displays the cumulative net permeation $\dot{N}_i^{perm}(A_k)$ along the area A_k of each membrane for the design points A-F. The cumulative net permeation $\dot{N}_i^{perm}(A_k)$ is calculated using Eq. (16) for each membrane unit. The sign convention is chosen in accordance with Eq. (6) and expresses the direction of permeation, with negative values indicating permeation from the retentate to the permeate side (into the sweep), while positive values indicate permeation from the permeate to the retentate side (out of the sweep). The membrane area A_k is defined as positive on the retentate side, again consistent with the sign convention used in Eq. (6). Note that the sweep side operates in counter-current mode and thus flows in the opposite direction from right to left.

$$\dot{N}_i^{perm}(A_k) = \sum_{j=1}^{k} -J_{i,j} \cdot \Delta A_j \tag{16}$$

Horizontal dashed lines in Fig. 4 indicate the feed flows of H_2O and MeOH to each membrane (retentate side), thus representing their maximum removable amounts in each separation step.

As the general results revealed significant differences in total specific compressor power and total specific heat transfer among the reference, condensation, and membrane process, the individual contributions to these indicators are detailed in Fig. 5 for the selected design points in Table 5. Fig. 5(a) shows the distribution of compressor power demands, while Fig. 5(b) presents the distribution of heating ($\dot{Q}_i > 0$) and cooling ($\dot{Q}_i < 0$) duties.

Selecting a high sweep pressure of $p_{Sweep} = 70\,bar$ (design case A) results in a weak driving force for product separation across the membrane. Consequently, the partial pressure gradients for MeOH and H_2O cannot be maintained along the entire membrane, leading to early sweep stream saturation in counter-current operation (Fig. 4A). As a result, a considerable portion of the membrane becomes ineffective. This leads to poor product removal, shown by the remaining distances to the dashed lines in Fig. 4A that represent the maximum removable amounts of MeOH and H_2O, respectively. Consequently, MeOH and H_2O accumulate in the process recycle, resulting in low single-pass conversion due to worse equilibrium and low carbon efficiency due to losses in the purge (Table 5). Additionally, the power consumption of the recycle compressor increases (Fig. 5(a)). Significant H_2 permeation from the sweep to the process side supplies hydrogen to the reaction, minimizing sweep-side compressor requirements (Fig. 5(a)). This effect of H_2 supply through the membrane is further discussed in Section 4.

A lower sweep pressure of $p_{Sweep} = 65\,bar$ (design case B) is able to maintain a strong and consistent driving force along the entire membrane, leading to an effective removal of nearly all H_2O and most MeOH (Fig. 4B). This increases single-pass conversion (Table 5) and lowers the power demand of the recycle compressor (Fig. 5(a)). While the power consumption of the H_2 compressor is reduced, less H_2 is supplied through the membrane to the reaction (Fig. 4B), increasing the power demand of the sweep-related compressors (Fig. 5(a)).

To further enhance product separation, the sweep pressure is lowered to $p_{Sweep} = 55\,bar$ (design case C). This enables near-complete removal of H_2O and MeOH in each stage. The process side is rapidly depleted from products and a large portion of the membrane remains

Table 5
Selected design cases for $p_{\mathrm{Process}} = 80\,\mathrm{bar}$ ($N = 3$, $\Delta p_{p,r}^{(n)} = 0.5\,\mathrm{bar}$, $A^{(n)} = 6000\,\mathrm{m^2}$).

	Ref.	Cond.	Membrane					
			A	B	C	D	E	F
N/-	1	3	3	3	3	3	3	3
p_{Process}/bar	80	80	80	80	80	80	80	80
p_{Sweep}/bar	–	–	70	65	55	65	65	65
ξ_{StP}/-	–	–	0.10	0.10	0.10	0.17	0.10	0.03
$\dot{N}_{③}$/kmol h^{-1}	51	20	32	22	19	28	32	21
$\dot{N}_{④}$/kmol h^{-1}	326	341	334	339	341	334	339	340
$y_{④,\mathrm{H_2O}}$/%	49.9	49.9	50.0	50.0	50.0	50.0	50.0	50.0
$y_{④,\mathrm{MeOH}}$/%	49.5	49.7	49.7	49.8	49.9	49.8	49.8	49.8
$X_{\mathrm{CO_2,SP}}$/%	30.3	75.0	45.5	52.9	68.3	44.3	52.9	63.6
η_{C}/%	93.9	98.5	96.6	98.3	98.9	96.6	98.3	98.5
$e_{\mathrm{comp,total}}$/ $\frac{\mathrm{kJ}}{\mathrm{mol}_{①,\mathrm{CO_2}}}$	27.5	26.5	28.2	27.1	29.5	28.2	27.1	29.0
$\frac{\mathrm{kJ}}{\mathrm{mol}_{④,\mathrm{MeOH}}}$	29.3	26.9	29.2	27.6	29.8	29.2	27.6	29.4
q_{total}/ $\frac{\mathrm{MJ}}{\mathrm{mol}_{①,\mathrm{CO_2}}}$	0.29	0.37	0.33	0.34	0.52	0.32	0.34	0.75
$\frac{\mathrm{MJ}}{\mathrm{mol}_{④,\mathrm{MeOH}}}$	0.31	0.38	0.34	0.35	0.51	0.33	0.35	0.76

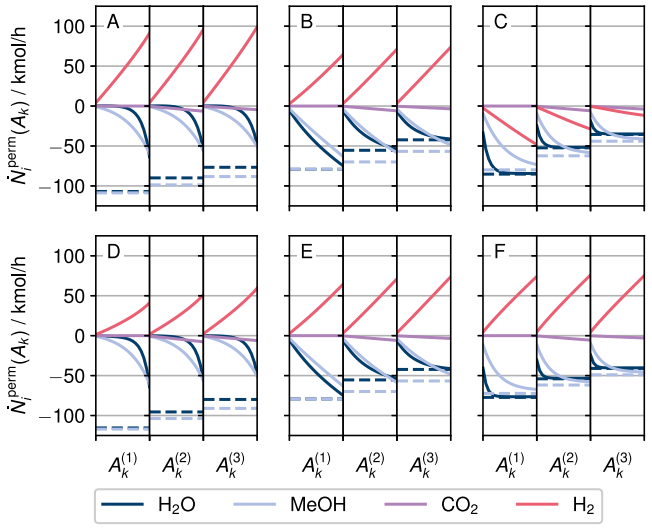

Fig. 4. Cumulative net permeation $\dot{N}_i^{\mathrm{perm}}(A_k)$ along the area A_k of each membrane for different designs A-F (see Table 5) of the membrane process ($N = 3$, $\Delta p_{p,r}^{(n)} = 0.5\,\mathrm{bar}$, $A^{(n)} = 6000\,\mathrm{m^2}$) at $p_{\mathrm{Process}} = 80\,\mathrm{bar}$. Dashed lines indicate the maximum removable amount of MeOH and H_2O, respectively.

unused (Fig. 4C). Single-pass conversion and carbon efficiency improve considerably (Table 5). Additionally, the H_2 compressor power demand is further reduced (Fig. 5(a)). However, the direction of H_2 permeation reverses, causing substantial H_2 permeation into the sweep. This drastically increases the load on both sweep compressors, particularly the sweep-to-process unit, which must now supply all H_2 to the reaction while additionally overcoming a growing pressure difference.

Similarly, varying the sweep-to-process split ξ_{StP} significantly affects the process performance. With a fixed H_2 feed ②, higher values of ξ_{StP} (design case D) reduce the sweep-side recirculation, as indicated by the lower duty of the sweep-to-sweep compressor (Fig. 5(a)). The resulting lower sweep flow rate leads to early saturation with H_2O and MeOH due to increased partial pressures in the sweep (Fig. 4D). At the same time, the H_2 partial pressure in the sweep decreases, reducing the H_2 supply for the reaction through the membrane. Together, these effects lower single-pass conversion and carbon efficiency (Table 5). In contrast, decreasing ξ_{StP} (design case F) increases the sweep flow rate, which dilutes H_2O and MeOH in the sweep, thereby enhancing separation (Fig. 4F) and improving single-pass conversion and carbon efficiency (Table 5). However, this benefit comes at the cost of increased sweep recirculation, raising the power demand of the sweep-to-sweep compressor (Fig. 5(a)).

In the condensation process, heating and cooling demands are higher than in the reference case, with heating duties evenly distributed and cooling duties decreasing along successive stages. In contrast, the membrane process design points exhibit reduced inter-reactor heat duties, as reactor effluents are only cooled down to 200 °C. However, these savings are offset by new thermal demands on the sweep-handling subsystem, as separated products must still be removed from the sweep itself via condensation. As a result, heat exchange is not eliminated in the membrane process but redistributed, and the total specific heat transfer is strongly influenced by the sweep configuration. Specifically, sweep pressure p_{Sweep} and sweep-to-process split ξ_{StP} significantly affect the distribution of heating and cooling duties (Fig. 5(b)). Reducing p_{Sweep} from design point A to C lowers heat transfer requirements between reactors due to improved single-pass conversion and lower flow through the reaction-separation stages but substantially increases sweep-side heat exchange, eventually exceeding that of the condensation process when H_2 permeates into the sweep. Decreasing ξ_{StP} from design point C to F directly increases sweep recirculation. The resulting enhancement in product removal and single-pass conversion initially reduces heat exchange between the reactors, similar to the effect of lower p_{Sweep}. However, as sweep recirculation continues to increase, the associated thermal load in the sweep-handling subsystem rises sharply, eventually dominating the overall heat exchange demand.

The analysis of the detailed design cases confirms that both sweep pressure p_{Sweep} and sweep-to-process split ξ_{StP} directly affect the transmembrane driving force, i.e., the partial pressure difference of permeating components in Eq. (10), as similarly reported by Hauth et al. [81]. Considering the permeate-side (sweep-side) partial pressures $p_{i,p}$,

$$p_{i,p} = \frac{\dot{N}_{i,p}}{\dot{N}_p(\xi_{\mathrm{StP}})} \cdot p_{\mathrm{Sweep}}, \tag{17}$$

this driving force is modulated either by the total pressure (p_{Sweep}) or by dilution/enrichment via the permeate (sweep) flow $\dot{N}_p(\xi_{\mathrm{StP}})$ as a function of ξ_{StP}. The process-level trade-offs between carbon efficiency η_{C}, total specific compressor power $e_{\mathrm{comp,total}}$ and heat transfer q_{total}, as shown in Fig. 3, are found to reflect competing requirements: minimizing H_2O and MeOH partial pressure and maximizing H_2 partial pressure on the permeate side of the membrane. In the best performing designs of the membrane process, this leads to bi-directional permeation, i.e., simultaneous removal of H_2O and MeOH and supply of H_2 through the membrane. Consequently, sweep conditions that yield low

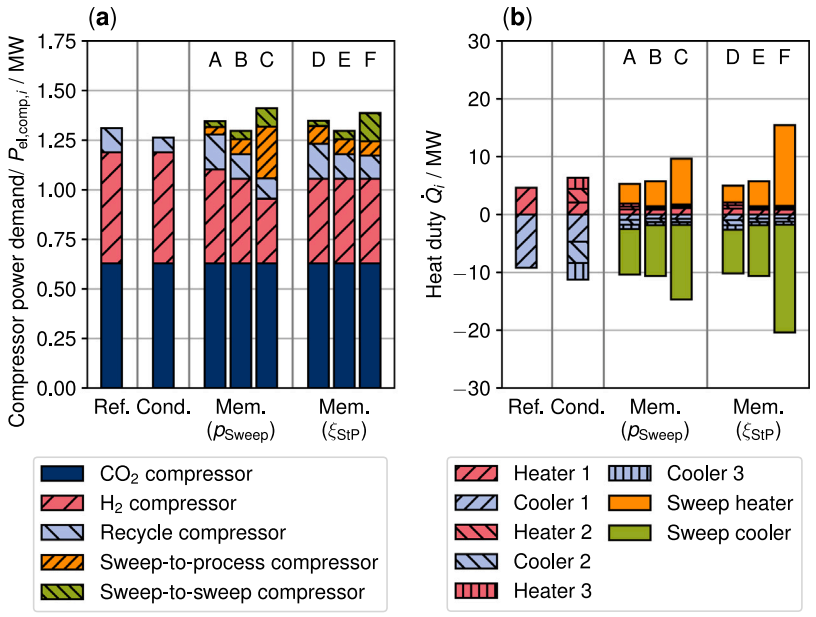

Fig. 5. Distribution of (a) compressor power demands and (b) heating ($\dot{Q}_i > 0$) and cooling ($\dot{Q}_i < 0$) for reference process (Ref.), condensation process (Cond.), and different designs A-F (Table 5) of the membrane process (Mem.) ($N = 3$, $\Delta p_{p,r}^{(n)} = 0.5\,\text{bar}$, $A^{(n)} = 6000\,\text{m}^2$) at $p_{\text{Process}} = 80\,\text{bar}$.

H_2 partial pressures, such as H_2-free sweep gas or very low sweep pressures, are impractical with current polymer membrane selectivities, as they either necessitate costly recompression of permeated H_2 or result in its loss. Component partial pressure curves for the different design cases A-F (see Table 5) of the membrane process are provided in the SI.

3.2. Scenarios

Furthermore, the influence of the number of reaction-separation stages N, the membrane module parameters (area $A^{(n)}$ and pressure drop $\Delta p_{p,r}^{(n)}$), and the membrane assumptions (H_2O/H_2 and H_2O/MeOH selectivities) on the performance metrics in Eqs. Eq. (12) to Eq. (14) has been investigated. To this end, the systematic variation of process pressure p_{Process}, sweep pressure p_{Sweep}, and sweep-to-process split ξ_{StP} within the ranges given in Table 3 is repeated for different numbers of separation stages N in Fig. 6, different membrane module areas $A^{(n)}$ and pressure drops $\Delta p_{p,r}^{(n)}$in Fig. 7, and different H_2O/H_2 and H_2O/MeOH selectivities in Fig. 8. Since each scenario results in a set of point clusters for the membrane process (cf. Fig. 3), only selected membrane design points are shown in the remainder of this work to illustrate the trends. These design points are chosen as the points on the Pareto-like front (cf. dashed line in Fig. 3) of each cluster that have the minimum relative distance (based on η_C and $e_{\text{comp,total}}$) to the corresponding condensation process design point at the same process pressure p_{Process}.

3.2.1. Stages

For both, condensation and membrane process, increasing the number of reaction-separation stages N generally results in improved product removal, a lower loop flow, and thus higher carbon efficiency η_C (Fig. 6). The associated cost in terms of total specific compressor power $e_{\text{comp,total}}$ and heat transfer q_{total} varies, however, significantly with the process pressure p_{Process} and the type of separation. For both processes, the incremental improvement from four to five stages is marginal at $p_{\text{Process}} = 60$ to $100\,\text{bar}$, suggesting that four stages represent a practical upper limit.

In the condensation process, the benefit of enhanced carbon efficiency η_C is accompanied by a systematic rise in total specific heat transfer q_{total} due to more frequent heating and cooling requirements.

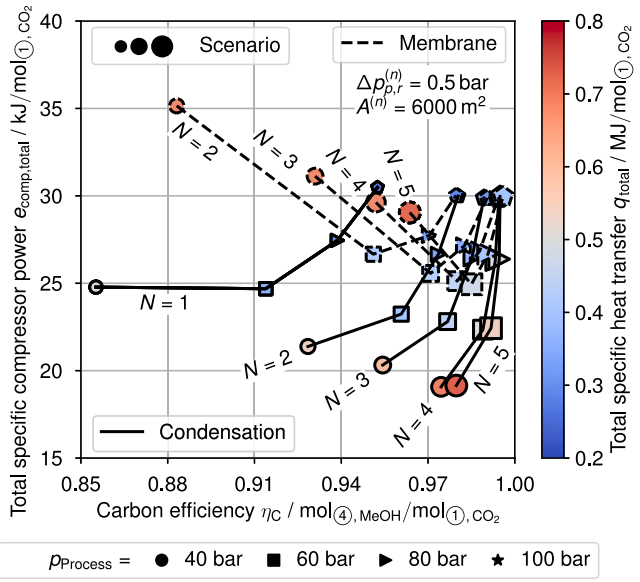

Fig. 6. Comparison of the reference, condensation, and selected membrane process design points for different numbers of reaction-separation stages N. Other parameters correspond to the base case values in Table 3.

At high process pressures, the positive effect of reduced recycle flow is largely offset by increased pressure losses, resulting in only minor changes in compressor power demand. In contrast, at low process pressures p_{Process}, the reduction in recycle flow leads to a more substantial decrease in total specific compressor power $e_{\text{comp,total}}$, improving overall process performance with additional stages. This results in a characteristic design trade-off between high-pressure operation with fewer stages and low-pressure operation with more stages. Within the medium-pressure range (60 bar to 80 bar), three stages can be seen as a practical optimum, beyond which further gains in carbon efficiency are expected to be marginal relative to the additional equipment-related costs.

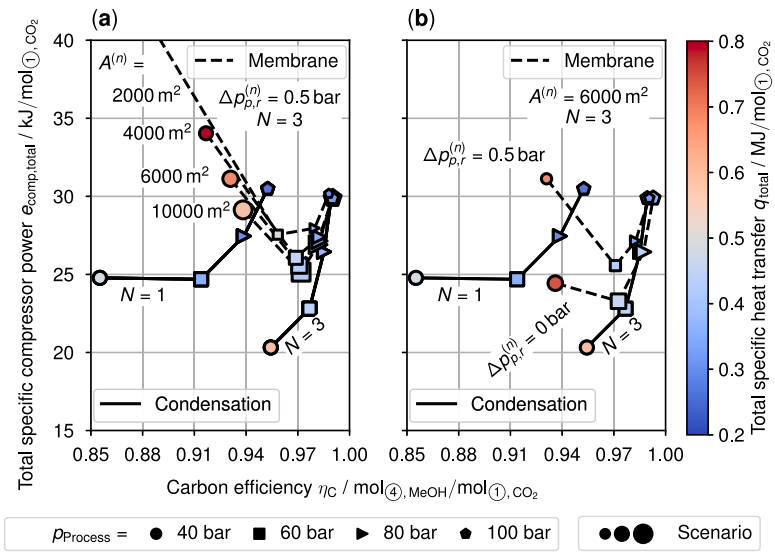

Fig. 7. Impact of (a) membrane area $A^{(n)}$ and (b) pressure drop $\Delta p_{p,r}^{(n)}$. Other parameters correspond to the base case values in Table 3.

The membrane process does not exhibit the same trade-off as the condensation process. Although increasing the number of stages reduces loop flow and lowers compressor power demand, membrane performance remains substantially inferior to the condensation process at low process pressure $p_{Process}$. With increasing process pressure $p_{Process}$, the performance gap narrows, particularly at higher stage numbers N. However, even at high stages numbers, parity with the condensation process is only reached at very high pressures (100 bar), which is energetically unfavorable in view of the modest gains in carbon efficiency relative to the substantial increase in compressor power demand. As previously identified in Fig. 5(b), the associated advantage of lower heat transfer q_{total} is marginal, as the thermal load is not eliminated but shifted to the sweep-handling subsystem of the membrane process.

3.2.2. Membrane assumptions

As already hinted at in Section 3.1, variations in membrane area $A^{(n)}$ primarily affect process performance at low process pressures (Fig. 7(a)) due to the small driving force for MeOH separation. Assuming constant membrane selectivities (Table 2), process performance can be significantly improved by an increasing membrane area. At higher process pressures, however, the benefit diminishes. In the medium-pressure range (60 bar to 80 bar), performance gains plateau between 4000 m² to 6000 m² for the considered plant scale. Further increases in membrane area yield negligible improvement.

To assess the impact of membrane pressure drop, pressure drops $\Delta p_{p,r}^{(n)}$ on both permeate and retentate sides are set to zero as an extreme case. The results in Fig. 7(b) indicate that particularly the compressor power demand is sensitive to the pressure drop within the membrane modules, emphasizing the importance of their hydraulic design. This effect is most pronounced at low process pressures and high recycle flow rates, where eliminating the pressure drop reduces the recycle compressor power significantly.

Finally, the influence of membrane permeabilities is investigated by varying the H_2O/H_2 in Fig. 8(a) and H_2O/MeOH selectivities in Fig. 8(b). Lower H_2O/H_2 selectivity, i.e., increased H_2 permeability, results in a slight decrease in compressor power demand in Fig. 8(a). As the presented design points correspond to sweep conditions with bi-directional permeation, this higher H_2 permeability allows to increasingly bypass the mechanical compression of H_2 in the sweep-to-process compressor (cf. Fig. 2) via transport through the membranes. In contrast, carbon efficiency declines. The stepwise H_2 introduction in subsequent reaction stages reduces its excess in the first reactor stage, lowering conversion and increasing recycle and purge losses. This effect diminishes at higher pressures, where equilibrium already favors conversion. Overall, the effect of H_2O/H_2 on process performance remains small due to the employed configuration of using the make-up H_2 as sweep. Consequently, H_2O/H_2 selectivity requirements could be relaxed to ranges achievable with current polymer membranes as shown in Fig. 1(b). This conclusion, however, depends on the membrane's ability of bi-directional permeation: if back-permeation were not possible, the benefit of reduced make-up H_2 compression (see Fig. 5(a)) would be lost and additional recompression would be required. The aspect of bi-directional permeation is further discussed in Section 4.

Variation of H_2O/MeOH selectivity in Fig. 8(b) has a more pronounced effect for the investigated process: higher selectivity, i.e., reduced MeOH permeation impairs performance, particularly at low process pressures where unfavorable equilibrium results in low MeOH partial pressures. Thus, higher MeOH permeance would be beneficial under these conditions, with an effect comparable to increasing membrane area (cf. Fig. 7(a)).

4. Discussion

The condensation process seems conceptually simple, as its product removal ability and thus performance is determined by vapor–liquid equilibrium, which in turn is mainly influenced by conventional design parameters such as process pressure and separator temperature. In contrast to the membrane process, the condensation process does not require costly additional compression stages, as the majority of hydrogen remains at high pressure at every product removal stage. However, practical equipment design might be challenging due to the close integration and proximity of reaction, heat transfer and separation units. The stage variation results in Fig. 6 show that the associated cooling and reheating demands increase total heat duty by 13 to 83 % in comparison to the single-stage reference (ranging from a single additional stage at $p_{Process}$ = 40 bar up to five stages at $p_{Process}$ = 100 bar). If these heat transfer and separation units are located outside the reactor pressure shell, as proposed by Banister et al. [26], Gal et al. [30], and Hillestad [29], the design is likely to require increased piping effort, multiple mechanically demanding high-pressure and high-temperature connections to the reactor shell, and independent pressure resistance for each unit. Conversely, integrating the reaction, heat transfer, and separation units within a single common pressure shell to avoid aforementioned drawbacks, as proposed by Castillo-Welter et al. [23], introduces other engineering challenges, such as unfavorable shell dimensions, difficulty in maintaining precise

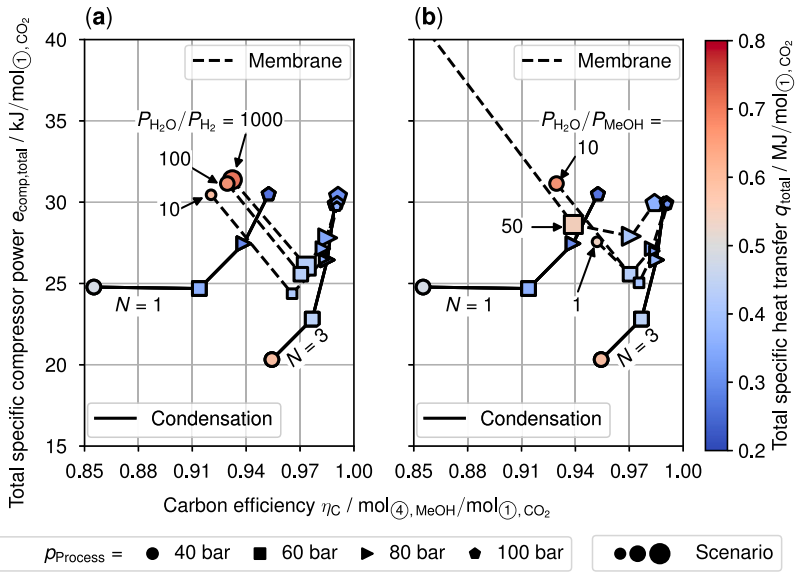

Fig. 8. Impact of membrane selectivities (a) P_{H_2O}/P_{H_2} and (b) P_{H_2O}/P_{MeOH}. Other parameters correspond to the base case values in Table 3.

temperature control due to the direct proximity of hot reaction zone to the cold separation zone, and thermal stresses arising from temperature gradients [32]. As the condensation concept can be realized through fundamentally different equipment arrangements, each with distinct complexity and cost implications, the present work should be understood as a conceptual screening study. In future work, the high performance of interstage condensation reported here should therefore be contextualized through a techno-economic evaluation that accounts for these equipment aspects, ideally across plant scales.

The membrane process exhibits higher conceptual complexity than the condensation process, as product removal and performance depend on a larger number of interdependent design parameters and require the introduction of sweep-handling equipment, as described in detail in Section 3.1.2. This complexity may, however, create further opportunities for systematic process optimization, for instance through the use of frameworks coupling process simulators with local optimization algorithms [82]. Some membrane process design points approach the performance of the condensation, e.g., at $p_{Process}$ = 80 bar and N = 3 for p_{Sweep} = 65 bar and ξ_{StP} = 0.1. Comparing this design point to interstage condensation at $p_{Process}$ = 80 bar and N = 3, compressor power demand is 2 % higher, total heat duty is 8 % lower, and carbon efficiency is slightly reduced from 98.5 % to 98.3 %. Our findings show that these membrane process design points exhibit bi-directional permeation across the membranes: H_2 is supplied from the sweep to the reaction side, while, at the same time, H_2O and MeOH permeate in the opposite direction into the sweep. This behavior was also reported by Dieterich et al. [61] for their MR COMP process design (sweep at synthesis pressure). However, since they considered an additional H_2 feed for the sweep, the need to compress it to synthesis pressure proved economically infeasible. As a result, they adopted an atmospheric sweep, similar to Hamedi et al. [60], and deduced that membranes must exhibit very low H_2 permeance, while maintaining stability to pressure differences of 50 bar to 100 bar. In contrast, the findings of this work suggest that bi-directional permeation could permit higher sweep pressures, thereby relaxing selectivity requirements to levels achievable with current polymer membranes, as confirmed in Fig. 8, and reducing constraints on membrane pressure resistance. However, it should be noted that ideal permeation behavior is assumed in this study. Real component permeances exhibit non-ideal behavior and depend on temperature, pressure and gas composition [83]. Especially for vapor permeation in polymer membranes, this further includes effects such as swelling, plasticization, and competitive sorption [84,85]. Further, flux coupling between permeating species [86] is not included in the model, which could become significant under conditions of bi-directional permeation. However, much of the available experimental permeation data in the context of methanol synthesis, as summarized in Fig. 1, has been obtained under conditions that differ substantially from conditions in this study in terms of temperature, pressure and gas composition. Beyond permeation behavior, membrane stability and integrity are critical operational concerns that could not be investigated in this study due to the absence of suitable models and data. These aspects should be a primary focus of future experimental work alongside permeability and selectivity characterization under realistic operating conditions.

5. Summary and outlook

In this work, we investigated interstage product separation strategies for CO_2-based methanol synthesis to overcome the equilibrium limitation, comparing condensation and polymer membrane units against a single-stage condensation process as reference. The evaluation was conducted from a process perspective, considering the synthesis loop to capture effects beyond the reactor level across a range of key process parameters.

Interstage condensation significantly increased CO_2 single-pass conversion and carbon efficiency relative to the reference process, particularly at low process pressures. This revealed a trade-off between high-pressure operation with fewer stages and low-pressure operation with more stages. The condensation concept proved less complex than the membrane-based design, while generally offering superior performance. A key advantage is that H_2 remains largely in the gas phase at high pressure rather than being co-separated. However, condensing products between reaction units lead to considerable heat transfer with large temperature differences in direct proximity to reaction stages.

In contrast to integrated membrane reactors, membrane-based interstage separation decouples reaction and separation conditions, enabling the use of low-cost polymer membranes. The issue of H_2 co-permeation required the introduction of a sweep stream, for which the H_2 make-up feed was used. Due to the separation temperature of 200 °C, the membrane process showed reduced heat transfer demands between reactors in comparison to the condensation process, but shifted them to the sweep-handling part of the process. Product separation was found to be highly sensitive to the parameters directly influencing the driving force over the membrane, i.e., the sweep pressure p_{Sweep} and sweep flow, manipulated by the split ξ_{StP}. These parameters determined

process performance, governed by a trade-off between minimizing H_2O and MeOH partial pressures and maximizing H_2 partial pressure on the permeate (sweep) side of the membranes. While aggressive separation conditions (very low sweep pressure, very high sweep flow) could surpass the carbon efficiency of the condensation process, they imposed an unacceptable increase in energetic and heat transfer burden in the sweep-handling part of the process. This finding highlights the importance of assessing such intensification strategies at the process level to prevent overlooking trade-offs and the shifting of burdens between subsystems. Milder sweep conditions (elevated sweep pressure and flow) resulted in bi-directional permeation, i.e., H_2 supply from the sweep to the reaction side, while simultaneously removing H_2O and MeOH in the opposite direction. This reduced the demand of upstream H_2 compression without compromising carbon efficiency and could be achieved with H_2O/H_2 selectivities in the range of current polymer membranes. However, the feasibility of bi-directional permeation of polymer membranes under real operating conditions remains to be experimentally demonstrated. Even in these cases, the condensation process remained the superior option.

From the comparison of process concepts in this study, interstage condensation emerges as the recommended strategy for addressing equilibrium limitations in CO_2-based methanol synthesis. However, the associated additional equipment warrants a more detailed techno-economic comparison and the need to address equipment-related challenges, e.g. the mechanical arrangement of equipment with large temperature differences in a common pressure shell. For smaller-scale Power-to-X applications, the additional investment cost from more equipment may weigh heavily, but the absence of scale limitations on equipment sizing could make the operational benefits particularly attractive. Future work should therefore combine process performance analysis (e.g. via exergy analysis) with realistic equipment design considerations to translate the demonstrated potential into practical and economically viable systems.

Abbreviations

ATE	Approach to equilibrium
Cond.	Condensation process
Mem.	Membrane process
Ref.	Reference process

Nomenclature

Variables

A	Membrane area	m^2
a_{1-7}	Polynomial parameters	–
b_{1-7}	Polynomial parameters	–
e	Specific power demand	$kJ\,mol^{-1}$
f_i	Fugacity of component i	bar
$\bar{H}_i$	Molar enthalpy of component i	$kJ\,mol^{-1}$
$\Delta\bar{H}_R^0$	Standard molar enthalpy of reaction	$kJ\,mol^{-1}$
J_i	Trans-membrane flux of component i	$kmol\,h^{-1}\,m^{-2}$
K_f	Equilibrium constant	–
$\dot{N}$	Molar flow	$kmol\,h^{-1}$
$\dot{N}_i$	Molar flow of component i	$kmol\,h^{-1}$
N	Number of reaction-separation stages	–
P_i	Permeance of component i	$mol\,m^{-2}\,s^{-1}\,Pa^{-1}$
P_{el}	Electrical power demand	kW
p	Pressure	bar
p_i	Partial pressure of component i	bar
p^0	Reference pressure	bar
Δp	Pressure drop	bar
$\dot{Q}$	Heat duty	kW
q	Specific heat transfer	$MJ\,mol^{-1}$
$\bar{R}$	Ideal gas constant	$J\,mol^{-1}\,K$
SN	Stoichiometric number	–
T	Temperature	°C, K
U_{mem}	Overall heat transfer coefficient of membrane	$W\,m^{-2}\,K^{-1}$
X	Conversion	–
y_i	Molar fraction of component i	–
η_C	Carbon efficiency	–
η_{is}	Isentropic efficiency	–
ν	Stoichiometric coefficient	–
ξ	Split factor	–

Subscripts

comp	Compressor
HCU	Heater/cooler unit
in	Inlet
j	Discretization step
k	Counter
out	Outlet
p	Permeate side
r	Retentate side
StP	Sweep-to-process
SP	Single-pass

Superscripts

(n)	Reaction/separation stage

CRediT authorship contribution statement

Matthias Schiedeck: Writing – review & editing, Writing – original draft, Methodology, Investigation, Conceptualization. **Hannes Stadler:** Writing – review & editing, Supervision, Methodology, Conceptualization. **Andreas Peschel:** Writing – review & editing, Supervision, Conceptualization.

Declaration of Generative AI and AI-assisted technologies in the manuscript preparation process

During the preparation of this work the authors used DeepL and ChatGPT-5 in order to improve the quality of writing in terms of grammatical correctness and stylistics. After using these tools, the authors reviewed and edited the content as needed and take full responsibility for the content of the published article.

Declaration of competing interest

The authors declare that they have no known competing financial interests or personal relationships that could have appeared to influence the work reported in this paper.

Acknowledgments

The authors acknowledge the funding by the German Federal Ministry of Research, Technology and Space (BMFTR), Germany and the Ministry of Economic Affairs, Industry, Climate Action and Energy of the State of North Rhine-Westphalia, Germany through the project HC-H2.

Appendix A. Supplementary data

Supplementary material related to this article can be found online at https://doi.org/10.1016/j.ceja.2026.101255.

Data availability

No data was used for the research described in the article.

References

[1] M. Weikl, A. Peschel, Industrial view on hydrogen carriers for intercontinental transport, Curr. Opin. Green Sustain. Chem. 44 (2023) 100843, http://dx.doi.org/10.1016/j.cogsc.2023.100843.

[2] A. Peschel, P. Wasserscheid, Perspective on the technology status of chemical hydrogen carriers for ship-based energy import, Electrochem. Sci. Adv. 6 (1) (2026) e70015, http://dx.doi.org/10.1002/elsa.70015.

[3] F. Nestler, M. Krüger, J. Full, M.J. Hadrich, R.J. White, A. Schaadt, Methanol synthesis–industrial challenges within a changing raw material landscape, Chem. Ing. Tech. 90 (10) (2018) 1409–1418, http://dx.doi.org/10.1002/cite.201800026.

[4] V. Dieterich, A. Buttler, A. Hanel, H. Spliethoff, S. Fendt, Power-to-liquid via synthesis of methanol, DME or Fischer–Tropsch-fuels: a review, Energy Environ. Sci. 13 (10) (2020) 3207–3252, http://dx.doi.org/10.1039/D0EE01187H.

[5] G.A. Olah, A. Goeppert, G.S. Prakash, Beyond Oil and Gas: the Methanol Economy, John Wiley & Sons, 2011.

[6] M.B. Fichtl, D. Schlereth, N. Jacobsen, I. Kasatkin, J. Schumann, M. Behrens, R. Schlögl, O. Hinrichsen, Kinetics of deactivation on Cu/ZnO/Al2o3 methanol synthesis catalysts, Appl. Catal. A: Gen. 502 (2015) 262–270, http://dx.doi.org/10.1016/j.apcata.2015.06.014.

[7] B. Lacerda de Oliveira Campos, K. John, P. Beeskow, K. Herrera Delgado, S. Pitter, N. Dahmen, J. Sauer, A detailed process and techno-economic analysis of methanol synthesis from H2 and CO2 with intermediate condensation steps, Processes 10 (8) (2022) 1535, http://dx.doi.org/10.3390/pr10081535.

[8] C. Xu, Z. Yan, J. Yu, X. Wang, H. Ban, Y. Wang, C. Li, Development of stable water-resistant Cu-based catalyst for methanol synthesis, Appl. Catal. A: Gen. 623 (2021) 118299, http://dx.doi.org/10.1016/j.apcata.2021.118299.

[9] N. Barrow, J. Bradley, B. Corrie, Y. Cui, T.D. Tran, T.E. Erden, A. Fish, M. Garcia, P. Glen, N. Mistry, et al., Doubling the life of Cu/ZnO methanol synthesis catalysts via use of Si as a structural promoter to inhibit sintering, Sci. Adv. 10 (3) (2024) eadk2081, http://dx.doi.org/10.1126/sciadv.adk2081.

[10] A. Arora, S.S. Iyer, I. Bajaj, M.F. Hasan, Optimal methanol production via sorption-enhanced reaction process, Ind. Eng. Chem. Res. 57 (42) (2018) 14143–14161, http://dx.doi.org/10.1021/acs.iecr.8b02543.

[11] M. Bayat, Z. Dehghani, M. Hamidi, M. Rahimpour, Methanol synthesis via sorption-enhanced reaction process: Modeling and multi-objective optimization, J. Taiwan Inst. Chem. Eng. 45 (2) (2014) 481–494, http://dx.doi.org/10.1016/j.jtice.2013.06.013.

[12] J. van Kampen, J. Boon, F. van Berkel, J. Vente, M. van Sint Annaland, Steam separation enhanced reactions: Review and outlook, Chem. Eng. J. 374 (2019) 1286–1303, http://dx.doi.org/10.1016/j.cej.2019.06.031.

[13] J.B. Hansen, P.E.H. Nielsen, Methanol synthesis, Handb. Heterog. Catal. (2008) 2920–2949.

[14] K. Westerterp, New methanol processes, in: Energy Efficiency in Process Technology, Springer, 1993, pp. 1142–1153.

[15] J. Reichert, S. Maerten, K. Meltzer, A. Tremel, M. Baldauf, P. Wasserscheid, J. Albert, Shifting the equilibrium of methanol synthesis from CO 2 by in situ absorption using ionic liquid media, Sustain. Energy Fuels 3 (12) (2019) 3399–3405, http://dx.doi.org/10.1039/C9SE00494G.

[16] J. Reichert, Entwicklung eines Prozesses zur Methanolsynthese mit kontinuierlicher Produktabtrennung durch in-situ Sorption, 2020.

[17] J. Ott, V. Gronemann, F. Pontzen, E. Fiedler, G. Grossmann, D.B. Kersebohm, G. Weiss, C. Witte, Methanol, Ullmann's Encycl. Ind. Chem. (2000) http://dx.doi.org/10.1002/14356007.a16_465.pub3.

[18] S.R. Early, Process for use in gas phase reactions, 2007, US7790775B2.

[19] S.R. Early, Method and system for the synthesis of methanol, 2007, US12202787B2.

[20] H.-J. Baehnisch, Verfahren und anlage zur methanolsynthese, 1992, EP0494350A2.

[21] Y. Kambe, K. Uchida, H. Watanabe, D. Hirakawa, T. Hasegawa, Methanolherstellungsverfahren und methanolherstellungsvorrichtung, 2021, EP3210961B1.

[22] G. Gabriele, Methanol process, 2024, GB2624544A.

[23] F. Castillo-Welter, S. Haag, R. Frind, T. Schuhmann, A. Ochs, M. Wagner, S. Valentin, Reactor for conducting exothermic equilibrium reactions, 2021, US10898874B2.

[24] C.P. van Dijk, L.D. Fraley, Process for recovering natural gas in the form of a normally liquid carbon containing compound, 1993, US5177114A.

[25] C.P. van Dijk, Methanol production process using a high nitrogen content synthesis gas with a hydrogen recycle, 1995, US5472986A.

[26] J.A. Banister, A.M. Johnston, B.S. Haynes, Multiple reactor chemical production system, 2011, US8075856B2.

[27] E. Moioli, R. Mutschler, A. Züttel, Renewable energy storage via CO2 and H2 conversion to methane and methanol: Assessment for small scale applications, Renew. Sustain. Energy Rev. 107 (2019) 497–506, http://dx.doi.org/10.1016/j.rser.2019.03.022.

[28] E. Moioli, A. Wötzel, T. Schildhauer, Feasibility assessment of small-scale methanol production via power-to-X, J. Clean. Prod. 359 (2022) 132071, http://dx.doi.org/10.1016/j.jclepro.2022.132071.

[29] M. Hillestad, Direct hydrogenation of carbon dioxide to methanol: Systematic generation of multi-stage designs, J. CO2 Util. 74 (2023) 102535, http://dx.doi.org/10.1016/j.jcou.2023.102535.

[30] E. Gal, R.M. Koros, B. Moskowitz, A. Keller, Multi-stage reactor and system for making methanol in a once-through process and methods therefor, 2018, US20180221842A1.

[31] S. Haag, C. Drosdzol, B. Williams, V. Peña, N. Palauschek, M. Wilken, A. Günther, V. Gronemann, A. Roesch, Recent developments in methanol technology by air liquide for CO2 reduction and CO2 usage, Chem. Ing. Tech. 94 (11) (2022) 1655–1666, http://dx.doi.org/10.1002/cite.202200061.

[32] M. Strozyk, F. Castillo-Welter, T. Oelmann, T. Schuhmann, Multistage reactor for performing exothermic equilibrium reactions, 2024, US20240066488A1.

[33] B. Williams, T. Schuhmann, V. Gronemann, S. Haag, F. Castillo-Welter, Process and plant for producing methanol from synthesis gases having a high proportion of carbon dioxide, 2020, US11078142B2.

[34] A. Schulz, N. Von Winning, S. Kunz, Method and system for the synthesis of methanol, 2020, US12404225B2.

[35] C. Wix, M. Boe, H.A. Helbo, Pseudo-isothermal reactor, 2015, US2017021322A1.

[36] R.P.W.J. Struis, S. Stucki, M. Wiedorn, A membrane reactor for methanol synthesis, J. Membr. Sci. 113 (1) (1996) 93–100, http://dx.doi.org/10.1016/0376-7388(95)00222-7.

[37] S.P. Nunes, P.Z. Culfaz-Emecen, G.Z. Ramon, T. Visser, G.H. Koops, W. Jin, M. Ulbricht, Thinking the future of membranes: Perspectives for advanced and new membrane materials and manufacturing processes, J. Membr. Sci. 598 (2020) 117761, http://dx.doi.org/10.1016/j.memsci.2019.117761.

[38] R.W. Baker, B.T. Low, Gas separation membrane materials: a perspective, Macromolecules 47 (20) (2014) 6999–7013, http://dx.doi.org/10.1021/ma501488s.

[39] Q.H. Pham, E. Goudeli, C.A. Scholes, Selective separation of water and methanol from hydrogen and carbon dioxide at elevated temperature through polyimide and polyimidazole based membranes, J. Membr. Sci. 686 (2023) 121990, http://dx.doi.org/10.1016/j.memsci.2023.121990.

[40] I. Elvira, J. Lasobras, J. Soler, J. Herguido, M. Menéndez, Preparation of polymeric-ceramic composite membranes for use in the methanol synthesis reaction, Front. Membr. Sci. Technol. 2 (2023) 1267374, http://dx.doi.org/10.3389/frmst.2023.1267374.

[41] A. Prašnikar, M. Linec, D.L. Jurković, D. Bajec, M. Sarić, B. Likozar, Understanding membrane-intensified catalytic CO2 reduction reactions to methanol by structure-based multisite micro-kinetic model, J. Clean. Prod. 463 (2024) 142480, http://dx.doi.org/10.1016/j.jclepro.2024.142480.

[42] G. Bargeman, F. van Berkel, M. den Exter, M. de Groot, H. Mengers, K. Nijmeijer, M. van Tuel, H. Vos, Process for separation methanol and water from non-condensables, 2016, EP2974785A1.

[43] G. Chen, Q. Yuan, Methanol synthesis from CO2 using a silicone rubber/ceramic composite membrane reactor, Sep. Purif. Technol. 34 (1–3) (2004) 227–237, http://dx.doi.org/10.1016/S1383-5866(03)00195-3.

[44] E. Juarez, J. Lasobras, J. Soler, J. Herguido, M. Menéndez, Polymer–ceramic composite membranes for water removal in membrane reactors, Membranes 11 (7) (2021) 472, http://dx.doi.org/10.3390/membranes11070472.

[45] M. Seshimo, B. Liu, H.R. Lee, K. Yogo, Y. Yamaguchi, N. Shigaki, Y. Mogi, H. Kita, S.-i. Nakao, Membrane reactor for methanol synthesis using Si-rich LTA zeolite membrane, Membranes 11 (7) (2021) 505, http://dx.doi.org/10.3390/membranes11070505.

[46] K. Sato, K. Sugimoto, Y. Sekine, M. Takada, M. Matsukata, T. Nakane, Application of FAU-type zeolite membranes to vapor/gas separation under high pressure and high temperature up to 5 MPa and 180 C, Microporous Mesoporous Mater. 101 (1–2) (2007) 312–318, http://dx.doi.org/10.1016/j.micromeso.2006.12.021.

[47] K.-I. Sawamura, T. Shirai, M. Takada, Y. Sekine, E. Kikuchi, M. Matsukata, Selective permeation and separation of steam from water–methanol–hydrogen gas mixtures through mordenite membrane, Catal. Today 132 (1–4) (2008) 182–187, http://dx.doi.org/10.1016/j.cattod.2007.12.005.

[48] G. Song, W. Zhou, C. Li, Z. Wang, F. Hu, T. Wang, Z. Li, A. Tang, M.P. Harold, S. Liu, et al., Semi-hollow LTA zeolite membrane for water permeation in simulated CO2 hydrogenation to methanol, J. Membr. Sci. 678 (2023) 121666, http://dx.doi.org/10.1016/j.memsci.2023.121666.

[49] R. Raso, M. Tovar, J. Lasobras, J. Herguido, I. Kumakiri, S. Araki, M. Menéndez, Zeolite membranes: Comparison in the separation of H2O/H2/CO2 mixtures and test of a reactor for CO2 hydrogenation to methanol, Catal. Today 364 (2021) 270–275, http://dx.doi.org/10.1016/j.cattod.2020.03.014.

[50] H. Li, C. Qiu, S. Ren, Q. Dong, S. Zhang, F. Zhou, X. Liang, J. Wang, S. Li, M. Yu, Na+-gated water-conducting nanochannels for boosting CO2 conversion to liquid fuels, Science 367 (6478) (2020) 667–671, http://dx.doi.org/10.1126/science.aaz6053.

[51] Y. Deng, Z. Li, T. Chen, Z. Bian, K. Lim, N. Dewangan, K.G. Haw, Z. Wang, S. Kawi, Low-cost and facile fabrication of defect-free water permeable membrane for CO2 hydrogenation to methanol, Chem. Eng. J. 435 (2022) 133554, http://dx.doi.org/10.1016/j.cej.2021.133554.

[52] F. Gallucci, Inorganic membrane reactors for methanol synthesis, in: Methanol, Elsevier, 2018, pp. 493–518, http://dx.doi.org/10.1016/B978-0-444-63903-5.00018-2.

[53] S. Poto, J.G. Endepoel, M.A. Llosa-Tanco, D.A. Pacheco-Tanaka, F. Gallucci, M.F.N. d'Angelo, Vapor/gas separation through carbon molecular sieve membranes: Experimental and theoretical investigation, Int. J. Hydrog. Energy 47 (21) (2022) 11385–11401, http://dx.doi.org/10.1016/j.ijhydene.2021.10.155.

[54] S. Richard, P. Olivier, M. Jegoux, C. Makhloufi, F. Gallucci, Membrane reactors technologies for e-fuel production & processing: A review, Int. J. Hydrog. Energy 112 (2025) 446–467, http://dx.doi.org/10.1016/j.ijhydene.2025.01.361.

[55] G. Barbieri, G. Marigliano, G. Golemme, E. Drioli, Simulation of CO2 hydrogenation with CH3oh removal in a zeolite membrane reactor, Chem. Eng. J. 85 (1) (2002) 53–59, http://dx.doi.org/10.1016/S1385-8947(01)00143-7.

[56] H. Hamedi, T. Brinkmann, Rigorous and customizable 1d simulation framework for membrane reactors to, in principle, enhance synthetic methanol production, ACS Sustain. Chem. Eng. 9 (22) (2021) 7620–7629, http://dx.doi.org/10.1021/acssuschemeng.1c01677.

[57] I.G. Iwakiri, C.V. Miguel, L.M. Madeira, Modeling and simulation of a steam-selective membrane reactor for power-to-methanol, Comput. Chem. Eng. 156 (2022) 107555, http://dx.doi.org/10.1016/j.compchemeng.2021.107555.

[58] R. Struis, S. Stucki, Verification of the membrane reactor concept for the methanol synthesis, Appl. Catal. A: Gen. 216 (1–2) (2001) 117–129, http://dx.doi.org/10.1016/S0926-860X(01)00548-8.

[59] E. Sjöberg, L. Sandström, J. Hedlund, Membrane processes for effective methanol synthesis in the forest based biorefinery, Catal. Today 156 (3–4) (2010) 87–92, http://dx.doi.org/10.1016/j.cattod.2010.02.037.

[60] H. Hamedi, T. Brinkmann, S. Shishatskiy, Membrane-assisted methanol synthesis processes and the required permselectivity, Membranes 11 (8) (2021) 596, http://dx.doi.org/10.3390/membranes11080596.

[61] V. Dieterich, N. Wein, H. Spliethoff, S. Fendt, Performance requirements of membrane reactors for the application in renewable methanol synthesis: A techno-economic assessment, Adv. Sustain. Syst. 6 (12) (2022) 2200254, http://dx.doi.org/10.1002/adsu.202200254.

[62] AVEVA Group Limited, AVEVA Process Simulation 2024.1, 2023, URL: https://www.aveva.com/en/products/process-simulation/.

[63] G. Soave, Equilibrium constants from a modified redlich-kwong equation of state, Chem. Eng. Sci. 27 (6) (1972) 1197–1203, http://dx.doi.org/10.1016/0009-2509(72)80096-4.

[64] R. Chauvy, D. Verdonck, L. Dubois, D. Thomas, G. De Weireld, Techno-economic feasibility and sustainability of an integrated carbon capture and conversion process to synthetic natural gas, J. CO2 Util. 47 (2021) 101488, http://dx.doi.org/10.1016/j.jcou.2021.101488.

[65] I.O. for Standardization, Hydrogen fuel quality - Product specification, ISO 14687:2025, International Organization for Standardization, Vernier, Geneva, Switzerland, 2025, URL: https://www.iso.org/standard/82660.html.

[66] G.H. Graaf, J.G. Winkelman, Chemical equilibria in methanol synthesis including the water–gas shift reaction: a critical reassessment, Ind. Eng. Chem. Res. 55 (20) (2016) 5854–5864, http://dx.doi.org/10.1021/acs.iecr.6b00815.

[67] N.D. Nielsen, A.D. Jensen, J.M. Christensen, The roles of CO and CO2 in high pressure methanol synthesis over Cu-based catalysts, J. Catalysis 393 (2021) 324–334, http://dx.doi.org/10.1016/j.jcat.2020.11.035.

[68] R.N. Nakashima, H. Nami, A. Nemati, G. Butera, P.V. Hendriksen, S. de Oliveira Junior, H.L. Frandsen, Integration of electrolysis with pyrolysis: effects of carbon conversion in methanol production, in: 7th International Conference on Contemporary Problems of Thermal Engineering, Silesian University of Technology, 2022, pp. 945–960.

[69] F. Nestler, A.R. Schütze, M. Ouda, M.J. Hadrich, A. Schaadt, S. Bajohr, T. Kolb, Kinetic modelling of methanol synthesis over commercial catalysts: A critical assessment, Chem. Eng. J. 394 (2020) 124881, http://dx.doi.org/10.1016/j.cej.2020.124881.

[70] G.H. Graaf, E.J. Stamhuis, A.A. Beenackers, Kinetics of low-pressure methanol synthesis, Chem. Eng. Sci. 43 (12) (1988) 3185–3195, http://dx.doi.org/10.1016/0009-2509(88)85127-3.

[71] L. Chen, Q. Jiang, Z. Song, D. Posarac, Optimization of methanol yield from a lurgi reactor, Chem. Eng. Technol. 34 (5) (2011) 817–822, http://dx.doi.org/10.1002/ceat.201000282.

[72] W.D. Seider, D.R. Lewin, J. Seader, S. Widagdo, R. Gani, K.M. Ng, Product and Process Design Principles: Synthesis, Analysis and Evaluation, John Wiley & Sons, 2017.

[73] B.A. Bishop, F.V. Lima, Modeling, simulation, and operability analysis of a nonisothermal, countercurrent, polymer membrane reactor, Processes 8 (1) (2020) 78, http://dx.doi.org/10.3390/pr8010078.

[74] A.J. Radcliffe, R.P. Singh, K.A. Berchtold, F.V. Lima, Modeling and optimization of high-performance polymer membrane reactor systems for water–gas shift reaction applications, Processes 4 (2) (2016) 8, http://dx.doi.org/10.3390/pr4020008.

[75] R. Turton, R.C. Bailie, W.B. Whiting, J.A. Shaeiwitz, Analysis, Synthesis and Design of Chemical Processes, Pearson Education, 2008.

[76] R. Checchetto, M.G. De Angelis, M. Minelli, Exploring the membrane-based separation of CO2/CO mixtures for CO2 capture and utilisation processes: Challenges and opportunities, Sep. Purif. Technol. 346 (2024) 127401, http://dx.doi.org/10.1016/j.seppur.2024.127401.

[77] C.E. Powell, G.G. Qiao, Polymeric CO2/N2 gas separation membranes for the capture of carbon dioxide from power plant flue gases, J. Membr. Sci. 279 (1–2) (2006) 1–49, http://dx.doi.org/10.1016/j.memsci.2005.12.062.

[78] G. Towler, R. Sinnott, Chemical Engineering Design: Principles, Practice and Economics of Plant and Process Design, Butterworth-Heinemann, 2021.

[79] S. Mbatha, X. Cui, P.G. Panah, S. Thomas, K. Parkhomenko, A.-C. Roger, B. Louis, R. Everson, P. Debiagi, N. Musyoka, et al., Comparative evaluation of the power-to-methanol process configurations and assessment of process flexibility, Energy Adv. 3 (9) (2024) 2245–2270, http://dx.doi.org/10.1039/D4YA00433G.

[80] M. Sadlowski, M. van Beek, Ecologic potential for flexible methanol production from steel mill off-gases, Chem. Ing. Tech. 92 (10) (2020) 1416–1424, http://dx.doi.org/10.1002/cite.202000085.

[81] T. Hauth, K. Pielmaier, V. Dieterich, N. Wein, H. Spliethoff, S. Fendt, Design parameter optimization of a membrane reactor for methanol synthesis using a sophisticated CFD model, Energy Adv. (2025) http://dx.doi.org/10.1039/D5YA00016E.

[82] J. Sundberg, S. Rehfeldt, A. Peschel, H. Klein, Prozessoptimierung am beispiel der methanolsynthese mithilfe verschiedener lokaler optimierungsalgorithmen, Chem. Ing. Tech. 5 (89) (2017) 675–685, http://dx.doi.org/10.1002/cite.201600108.

[83] E.S. Miandoab, S.E. Kentish, C.A. Scholes, Modelling competitive sorption and plasticization of glassy polymeric membranes used in biogas upgrading, J. Membr. Sci. 617 (2021) 118643, http://dx.doi.org/10.1016/j.memsci.2020.118643.

[84] C.A. Scholes, B.D. Freeman, S.E. Kentish, Water vapor permeability and competitive sorption in thermally rearranged (TR) membranes, J. Membr. Sci. 470 (2014) 132–137, http://dx.doi.org/10.1016/j.memsci.2014.07.024.

[85] G.Q. Chen, C.A. Scholes, C.M. Doherty, A.J. Hill, G.G. Qiao, S.E. Kentish, Modeling of the sorption and transport properties of water vapor in polyimide membranes, J. Membr. Sci. 409 (2012) 96–104, http://dx.doi.org/10.1016/j.memsci.2012.03.047.

[86] C. Castel, R. Bounaceur, E. Favre, Engineering of membrane gas separation processes: State of the art and prospects, J. Membr. Sci. Res. (2020) http://dx.doi.org/10.22079/JMSR.2020.123897.1363.